arXiv:0704.0807v1 [nucl-th] 5 Apr 2007

Nuclear Forces from Chiral Effective Field Theory*

R.Machleidt
Department of Physics, University of Idaho, Moscow, Idaho, U.S.A.

November 20, 2018

Abstract

In this lecture series, I present the recent progress in our understanding of nuclear forces in terms of chiral effective field theory.

Contents

1 Introduction and Historical Perspective **3**

2 QCD and the Nuclear Force **5**

3 Effective Field Theory for Low-Energy QCD **5**
3.1 Symmetries of Low-Energy QCD 6
3.1.1 Chiral Symmetry 6
3.1.2 Explicit Symmetry Breaking 9
3.1.3 Spontaneous Symmetry Breaking 9
3.2 Chiral Effective Lagrangians Involving Pions 10
3.3 Nucleon Contact Lagrangians 12

4 Nuclear Forces from EFT: Overview **13**
4.1 Chiral Perturbation Theory and Power Counting 14
4.2 The Hierarchy of Nuclear Forces 14

*Lecture series presented at the DAE-BRNS Workshop on Physics and Astrophysics of Hadrons and Hadronic Matter, Visva Bharati University, Santiniketan, West Bengal, India, November 2006.

5 Two-Nucleon Forces **16**
5.1 Pion-Exchange Contributions in ChPT 16
5.1.1 Zeroth Order (LO) 17
5.1.2 Second Order (NLO) 17
5.1.3 Third Order (NNLO) 19
5.1.4 Fourth Order (N^3LO) 20
5.1.5 Iterated One-Pion-Exchange 20
5.2 NN Scattering in Peripheral Partial Waves Using the Perturbative Amplitude 22
5.3 NN Contact Potentials 28
5.3.1 Zeroth Order 29
5.3.2 Second Order 30
5.3.3 Fourth Order 30
5.4 Constructing a Chiral NN Potential 31
5.4.1 Conceptual Questions 31
5.4.2 What Order? 33
5.4.3 Charge-Dependence 34
5.4.4 A Quantitative NN Potential at N^3LO 36

6 Many-Nucleon Forces **39**
6.1 Three-Nucleon Forces 40
6.2 Four-Nucleon Forces 42

7 Conclusions **42**

A Fourth Order Two-Pion Exchange Contributions **44**
A.1 One-loop diagrams 44
A.1.1 c_i^2 contributions. 44
A.1.2 c_i/M_N contributions. 44
A.1.3 $1/M_N^2$ corrections. 45
A.2 Two-loop contributions. 46

B Partial Wave Decomposition of the Fourth Order Contact Potential **48**

1 Introduction and Historical Perspective

The theory of nuclear forces has a long history (cf. Table 1). Based upon the seminal idea by Yukawa [1], first field-theoretic attempts to derive the nucleon-nucleon (NN) interaction focused on pion-exchange. While the one-pion exchange turned out to be very useful in explaining NN scattering data and the properties of the deuteron [2], multi-pion exchange was beset with serious ambiguities [3, 4]. Thus, the "pion theories" of the 1950s are generally judged as failures—for reasons we understand today: pion dynamics is constrained by chiral symmetry, a crucial point that was unknown in the 1950s.

Historically, the experimental discovery of heavy mesons [5] in the early 1960s saved the situation. The one-boson-exchange (OBE) model [6, 7] emerged which is still the most economical and quantitative phenomenology for describing the nuclear force [8, 9]. The weak point of this model, however, is the scalar-isoscalar "sigma" or "epsilon" boson, for which the empirical evidence remains controversial. Since this boson is associated with the correlated (or resonant) exchange of two pions, a vast theoretical effort that occupied more than a decade was launched to derive the 2π-exchange contribution to the nuclear force, which creates the intermediate range attraction. For this, dispersion theory as well as field theory were invoked producing the Stony Brook [10], Paris [11, 12], and Bonn [7, 13] potentials.

The nuclear force problem appeared to be solved; however, with the discovery of quantum chromodynamics (QCD), all "meson theories" were relegated to models and the attempts to derive the nuclear force started all over again.

The problem with a derivation from QCD is that this theory is non-perturbative in the low-energy regime characteristic of nuclear physics, which makes direct solutions impossible. Therefore, during the first round of new attempts, QCD-inspired quark models [14] became popular. These models are able to reproduce qualitatively and, in some cases, semi-quantitatively the gross features of the nuclear force [15, 16]. However, on a critical note, it has been pointed out that these quark-based approaches are nothing but another set of models and, thus, do not represent any fundamental progress. Equally well, one may then stay with the simpler and much more quantitative meson models.

A major breakthrough occurred when the concept of an effective field theory (EFT) was introduced and applied to low-energy QCD. As outlined by Weinberg in a seminal paper [17], one has to write down the most general Lagrangian consistent with the assumed symmetry principles, particularly

Table 1: Seven Decades of Struggle: The Theory of Nuclear Forces

1935	**Yukawa: Meson Theory**
1950's	*The "Pion Theories"* One-Pion Exchange: o.k. Multi-Pion Exchange: disaster
1960's	Many pions ≡ multi-pion resonances: $\boldsymbol{\sigma}$, $\boldsymbol{\rho}$, $\boldsymbol{\omega}$, ... The One-Boson-Exchange Model: success
1970's	Refined meson models, including sophisticated $\mathbf{2\pi}$ exchange contributions (Stony Brook, Paris, Bonn)
1980's	Nuclear physicists discover **QCD** Quark Cluster Models
1990's and beyond	Nuclear physicists discover **EFT** Weinberg, van Kolck **Back to Pion Theory!** *But, constrained by Chiral Symmetry: success*

the (broken) chiral symmetry of QCD. At low energy, the effective degrees of freedom are pions and nucleons rather than quarks and gluons; heavy mesons and nucleon resonances are "integrated out". So, the circle of history is closing and we are back to Yukawa's meson theory, except that we have learned to add one important refinement to the theory: broken chiral symmetry is a crucial constraint that generates and controls the dynamics and establishes a clear connection with the underlying theory, QCD.

Following the first initiative by Weinberg [18], pioneering work was performed by Ordóñez, Ray, and van Kolck [19, 20] who constructed a NN potential in coordinate space based upon chiral perturbation theory at next-to-next-to-leading order. The results were encouraging and many researchers became attracted to the new field [21, 22, 23, 24, 25, 26, 27]. As a consequence, nuclear EFT has developed into one of the most popular branches of modern nuclear physics [28, 29].

It is the purpose of these lectures to describe in some detail the recent

progress in our understanding of nuclear forces in terms of nuclear EFT.

2 QCD and the Nuclear Force

Quantum chromodynamics (QCD) is the theory of strong interactions. It deals with quarks, gluons and their interactions and is part of the Standard Model of Particle Physics. QCD is a non-Abelian gauge field theory with color $SU(3)$ the underlying gauge group. The non-Abelian nature of the theory has dramatic consequences. While the interaction between colored objects is weak at short distances or high momentum transfer ("asymptotic freedom"); it is strong at long distances ($\gtrsim 1$ fm) or low energies, leading to the confinement of quarks into colorless objects, the hadrons. Consequently, QCD allows for a perturbative analysis at large energies, whereas it is highly non-perturbative in the low-energy regime. Nuclear physics resides at low energies and the force between nucleons is a residual QCD interaction. Therefore, in terms of quarks and gluons, the nuclear force is a very complicated problem.

3 Effective Field Theory for Low-Energy QCD

The way out of the dilemma of how to derive the nuclear force from QCD is provided by the effective field theory (EFT) concept. First, one needs to identify the relevant degrees of freedom. For the ground state and the low-energy excitation spectrum of an atomic nucleus as well as for conventional nuclear reactions, quarks and gluons are ineffective degrees of freedom, while nucleons and pions are the appropriate ones. Second; to make sure that this EFT is not just another phenomenology, the EFT must observe all relevant symmetries of the underlying theory. This requirement is based upon a 'folk theorem' by Weinberg [17]:

> If one writes down the most general possible Lagrangian, including *all* terms consistent with assumed symmetry principles, and then calculates matrix elements with this Lagrangian to any given order of perturbation theory, the result will simply be the most general possible S-matrix consistent with analyticity, perturbative unitarity, cluster decomposition, and the assumed symmetry principles.

Thus, the EFT program consists of the following steps:

1. Identify the degrees of freedom relevant at the resolution scale of (low-energy) nuclear physics: nucleons and pions.
2. Identify the relevant symmetries of low-energy QCD and investigate if and how they are broken.
3. Construct the most general Lagrangian consistent with those symmetries and the symmetry breaking.
4. Design an organizational scheme that can distinguish between more and less important contributions: a low-momentum expansion.
5. Guided by the expansion, calculate Feynman diagrams to the the desired accuracy for the problem under consideration.

We will now elaborate on these steps, one by one.

3.1 Symmetries of Low-Energy QCD

In this section, we will give a brief introduction into (low-energy) QCD, its symmetries and symmetry breaking. A more detailed introduction can be found in the excellent lecture series by Scherer and Schindler [30].

3.1.1 Chiral Symmetry

The QCD Lagrangian reads

$$\mathcal{L}_{\mathrm{QCD}} = \bar{q}(i\gamma^\mu \mathcal{D}_\mu - \mathcal{M})q - \frac{1}{4}\mathcal{G}_{\mu\nu,a}\mathcal{G}_a^{\mu\nu} \tag{1}$$

with the gauge-covariant derivative

$$\mathcal{D}_\mu = \partial_\mu + ig\frac{\lambda_a}{2}\mathcal{A}_{\mu,a} \tag{2}$$

and the gluon field strength tensor

$$\mathcal{G}_{\mu\nu,a} = \partial_\mu \mathcal{A}_{\nu,a} - \partial_\nu \mathcal{A}_{\mu,a} - g f_{abc}\mathcal{A}_{\mu,b}\mathcal{A}_{\nu,c}\,. \tag{3}$$

In the above, q denotes the quark fields and $\mathcal{M}$ the quark mass matrix. Further, g is the strong coupling constant and $\mathcal{A}_{\mu,a}$ are the gluon fields. The λ_a are the Gell-Mann matrices and the f_{abc} the structure constants of the $SU(3)_{\mathrm{color}}$ Lie algebra $(a, b, c = 1, \ldots, 8)$; summation over repeated indices is always implied. The gluon-gluon term in the last equation arises

from the non-Abelian nature of the gauge theory and is the reason for the peculiar features of the color force.

On a typical hadronic scale, i.e., on a scale of low-mass hadrons which are not Goldstone bosons, e.g., $m_\rho = 0.78$ GeV ≈ 1 GeV; the masses of the up (u), down (d), and—to a certain extend—strange (s) quarks are small [31]:

$$m_u = 2 \pm 1 \text{ MeV} \tag{4}$$

$$m_d = 5 \pm 2 \text{ MeV} \tag{5}$$

$$m_s = 95 \pm 25 \text{ MeV} \tag{6}$$

It is therefore of interest to discuss the QCD Lagrangian in the limit of vanishing quark masses:

$$\mathcal{L}^0_{\text{QCD}} = \bar{q} i\gamma^\mu \mathcal{D}_\mu q - \frac{1}{4}\mathcal{G}_{\mu\nu,a}\mathcal{G}^{\mu\nu}_a \,. \tag{7}$$

Defining right- and left-handed quark fields,

$$q_R = P_R q \,, \quad q_L = P_L q \,, \tag{8}$$

with

$$P_R = \frac{1}{2}(1+\gamma_5) \,, \quad P_L = \frac{1}{2}(1-\gamma_5) \,, \tag{9}$$

we can rewrite the Lagrangian as follows:

$$\mathcal{L}^0_{\text{QCD}} = \bar{q}_R i\gamma^\mu \mathcal{D}_\mu q_R + \bar{q}_L i\gamma^\mu \mathcal{D}_\mu q_L - \frac{1}{4}\mathcal{G}_{\mu\nu,a}\mathcal{G}^{\mu\nu}_a \,. \tag{10}$$

Restricting ourselves now to up and down quarks, we see that $\mathcal{L}^0_{\text{QCD}}$ is invariant under the global unitary transformations

$$q_R = \begin{pmatrix} u_R \\ d_R \end{pmatrix} \longmapsto \exp\left(-i\Theta^R_i \frac{\tau_i}{2}\right) \begin{pmatrix} u_R \\ d_R \end{pmatrix} \tag{11}$$

and

$$q_L = \begin{pmatrix} u_L \\ d_L \end{pmatrix} \longmapsto \exp\left(-i\Theta^L_i \frac{\tau_i}{2}\right) \begin{pmatrix} u_L \\ d_L \end{pmatrix} \,, \tag{12}$$

where τ_i ($i = 1, 2, 3$) are the generators of $SU(2)_{\text{flavor}}$, the usual Pauli spin matrices. *The right- and left-handed components of massless quarks do not mix.* This is $SU(2)_R \times SU(2)_R$ symmetry, also known as *chiral symmetry.* Noether's Theorem implies the existence of six conserved currents; three right-handed currents

$$R^\mu_i = \bar{q}_R \gamma^\mu \frac{\tau_i}{2} q_R \quad \text{with} \quad \partial_\mu R^\mu_i = 0 \tag{13}$$

and three left-handed currents

$$L_i^\mu = \bar{q}_L \gamma^\mu \frac{\tau_i}{2} q_L \quad \text{with} \quad \partial_\mu L_i^\mu = 0\,. \tag{14}$$

It is useful to consider the following linear combinations; namely, three vector currents

$$V_i^\mu = R_i^\mu + L_i^\mu = \bar{q}\gamma^\mu \frac{\tau_i}{2} q \quad \text{with} \quad \partial_\mu V_i^\mu = 0 \tag{15}$$

and three axial-vector currents

$$A_i^\mu = R_i^\mu - L_i^\mu = \bar{q}\gamma^\mu \gamma_5 \frac{\tau_i}{2} q \quad \text{with} \quad \partial_\mu A_i^\mu = 0\,, \tag{16}$$

which got their names from the fact that they transform as vectors and axial-vectors, respectively. Thus, the chiral $SU(2)_L \times SU(2)_R$ symmetry is equivalent to $SU(2)_V \times SU(2)_A$, where the vector and axial-vector transformations are given respectively by

$$q = \begin{pmatrix} u \\ d \end{pmatrix} \longmapsto \exp\left(-i\Theta_i^V \frac{\tau_i}{2}\right) \begin{pmatrix} u \\ d \end{pmatrix} \tag{17}$$

and

$$q = \begin{pmatrix} u \\ d \end{pmatrix} \longmapsto \exp\left(-i\Theta_i^A \gamma_5 \frac{\tau_i}{2}\right) \begin{pmatrix} u \\ d \end{pmatrix}\,. \tag{18}$$

Obviously, the vector transformations are isospin rotations and, therefore, invariance under vector transformations can be identified with isospin symmetry.

There are the six conserved charges,

$$Q_i^V = \int d^3x\; V_i^0 = \int d^3x\; q^\dagger(t,\vec{x}) \frac{\tau_i}{2} q(t,\vec{x}) \quad \text{with} \quad \frac{dQ_i^V}{dt} = 0 \tag{19}$$

and

$$Q_i^A = \int d^3x\; A_i^0 = \int d^3x\; q^\dagger(t,\vec{x}) \gamma_5 \frac{\tau_i}{2} q(t,\vec{x}) \quad \text{with} \quad \frac{dQ_i^A}{dt} = 0\,, \tag{20}$$

which are also generators of $SU(2)_V \times SU(2)_A$.

3.1.2 Explicit Symmetry Breaking

The mass term $-\bar{q}\mathcal{M}q$ in the QCD Lagrangian Eq. (1) breaks chiral symmetry explicitly. To better see this, let's rewrite $\mathcal{M}$,

$$\mathcal{M} = \begin{pmatrix} m_u & 0 \\ 0 & m_d \end{pmatrix} \tag{21}$$

$$= \frac{1}{2}(m_u + m_d) \begin{pmatrix} 1 & 0 \\ 0 & 1 \end{pmatrix} + \frac{1}{2}(m_u - m_d) \begin{pmatrix} 1 & 0 \\ 0 & -1 \end{pmatrix} \tag{22}$$

$$= \frac{1}{2}(m_u + m_d)\, I + \frac{1}{2}(m_u - m_d)\, \tau_3 \,. \tag{23}$$

The first term in the last equation in invariant under $SU(2)_V$ (isospin symmetry) and the second term vanishes for $m_u = m_d$. Thus, isospin is an exact symmetry if $m_u = m_d$. However, both terms in Eq. (23) break $SU(2)_A$. Since the up and down quark masses are small as compared to the typical hadronic mass scale of ≈ 1 GeV [cf. Eqs. (4) and (5)], the explicit chiral symmetry breaking due to non-vanishing quark masses is very small.

3.1.3 Spontaneous Symmetry Breaking

A (continuous) symmetry is said to be *spontaneously broken* if a symmetry of the Lagrangian is not realized in the ground state of the system. There is evidence that the chiral symmetry of the QCD Lagrangian is spontaneously broken—for dynamical reasons of nonperturbative origin which are not fully understood at this time. The most plausible evidence comes from the hadron spectrum. From chiral symmetry, one would naively expect the existence of degenerate hadron multiplets of opposite parity, i.e., for any hadron of positive parity one would expect a degenerate hadron state of negative parity and vice versa. However, these "parity doublets" are not observed in nature. For example, take the ρ-meson, a vector meson with negative parity (1^-) and mass 776 MeV. There does exist a 1^+ meson, the a_1, but it has a mass of 1230 MeV and, thus, cannot be perceived as degenerate with the ρ. On the other hand, the ρ meson comes in three charge states (equivalent to three isospin states), the $\rho^\pm$ and the ρ^0 with masses that differ by at most a few MeV. In summary, in the QCD ground state (the hadron spectrum) $SU(2)_V$ (isospin symmetry) is well observed, while $SU(2)_A$ (axial symmetry) is broken. Or, in other words, $SU(2)_V \times SU(2)_A$ is broken down to $SU(2)_V$.

A spontaneously broken global symmetry implies the existence of (massless) Goldstone bosons with the quantum numbers of the broken generators. The broken generators are the Q_i^A of Eq. (20) which are pseudoscalar. The

Goldstone bosons are identified with the isospin triplet of the (pseudoscalar) pions, which explains why pions are so light. The pion masses are not exactly zero because the up and down quark masses are not exactly zero either (explicit symmetry breaking). Thus, pions are a truly remarkable species: they reflect spontaneous as well as explicit symmetry breaking.

3.2 Chiral Effective Lagrangians Involving Pions

The next step in our EFT program is to build the most general Lagrangian consistent with the (broken) symmetries discussed above. An elegant formalism for the construction of such Lagrangians was developed by Callan, Coleman, Wess, and Zumino (CCWZ) [32] who worked out the group-theoretical foundations of non-linear realizations of chiral symmetry. The Lagrangians given below are built upon the CCWZ formalism.

As discussed, the relevant degrees of freedom are pions (Goldstone bosons) and nucleons. Since the interactions of Goldstone bosons must vanish at zero momentum transfer and in the chiral limit ($m \to 0$), the low-energy expansion of the Lagrangian is arranged in powers of derivatives and pion masses. This is chiral perturbation theory (ChPT).

The Lagrangian consists of one part that deals with the interaction among pions, $\mathcal{L}_{\pi\pi}$, and another one that describes the interaction between pions and the nucleon, $\mathcal{L}_{\pi N}$:

$$\mathcal{L}_{\text{eff}} = \mathcal{L}_{\pi\pi} + \mathcal{L}_{\pi N} \tag{24}$$

with

$$\mathcal{L}_{\pi\pi} = \mathcal{L}_{\pi\pi}^{(2)} + \mathcal{L}_{\pi\pi}^{(4)} + \dots \tag{25}$$

and

$$\mathcal{L}_{\pi N} = \mathcal{L}_{\pi N}^{(1)} + \mathcal{L}_{\pi N}^{(2)} + \mathcal{L}_{\pi N}^{(3)} + \dots, \tag{26}$$

where the superscript refers to the number of derivatives or pion mass insertions (chiral dimension) and the ellipsis stands for terms of higher dimension.

The *leading order (LO)* $\pi\pi$ Lagrangian is given by [33]

$$\mathcal{L}_{\pi\pi}^{(2)} = \frac{f_\pi^2}{4} \operatorname{tr}\left[\, \partial^\mu U \partial_\mu U^\dagger + m_\pi^2 (U + U^\dagger) \,\right] \tag{27}$$

and the LO relativistic πN Lagrangian reads [34]

$$\mathcal{L}_{\pi N}^{(1)} = \bar{\Psi} \left(i\gamma^\mu D_\mu - M_N + \frac{g_A}{2} \gamma^\mu \gamma_5 u_\mu \right) \Psi \tag{28}$$

with

$$
\begin{aligned}
D_\mu &= \partial_\mu + \Gamma_\mu && (29)\\
\Gamma_\mu &= \frac{1}{2}(\xi^\dagger \partial_\mu \xi + \xi \partial_\mu \xi^\dagger) = \frac{i}{4f_\pi^2}\,\boldsymbol{\tau}\cdot(\boldsymbol{\pi}\times\partial_\mu\boldsymbol{\pi}) + \ldots && (30)\\
u_\mu &= i(\xi^\dagger \partial_\mu \xi - \xi \partial_\mu \xi^\dagger) = -\frac{1}{f_\pi}\,\boldsymbol{\tau}\cdot\partial_\mu\boldsymbol{\pi} + \ldots && (31)\\
U &= \xi^2 = 1 + \frac{i}{f_\pi}\boldsymbol{\tau}\cdot\boldsymbol{\pi} - \frac{1}{2f_\pi^2}\boldsymbol{\pi}^2 - \frac{i\alpha}{f_\pi^3}(\boldsymbol{\tau}\cdot\boldsymbol{\pi})^3 + \frac{8\alpha-1}{8f_\pi^4}\boldsymbol{\pi}^4 + \ldots && (32)
\end{aligned}
$$

In Eq. (28) the chirally covariant derivative D_μ is applied which introduces the "gauge term" Γ_μ (also known as chiral connection), a vector current that leads to a coupling of pions with the nucleon. Besides this, the Lagrangian includes a coupling term which involves the axial vector u_μ. The $SU(2)$ matrix $U = \xi^2$ collects the Goldstone pion fields.

In the above equations, M_N denotes the nucleon mass, g_A the axial-vector coupling constant, and f_π the pion decay constant. Numerical values will be given later.

The coefficient α that appears in Eq. (32) is arbitrary. Therefore, diagrams with chiral vertices that involve three or four pions must always be grouped together such that the α-dependence drops out (cf. Fig. 4, below).

We apply the heavy baryon (HB) formulation of chiral perturbation theory [35] in which the relativistic πN Lagrangian is subjected to an expansion in terms of powers of $1/M_N$ (kind of a nonrelativistic expansion), the lowest order of which is

$$
\begin{aligned}
\widehat{\mathcal{L}}^{(1)}_{\pi N} &= \bar{N}\left(iD_0 - \frac{g_A}{2}\,\vec{\sigma}\cdot\vec{u}\right)N\\
&= \bar{N}\left[i\partial_0 - \frac{1}{4f_\pi^2}\,\boldsymbol{\tau}\cdot(\boldsymbol{\pi}\times\partial_0\boldsymbol{\pi}) - \frac{g_A}{2f_\pi}\,\boldsymbol{\tau}\cdot(\vec{\sigma}\cdot\vec{\nabla})\boldsymbol{\pi}\right]N + \ldots \quad (33)
\end{aligned}
$$

In the relativistic formulation, the nucleon is represented by a four-component Dirac spinor field, Ψ, while in the HB version, the nucleon, N, is a Pauli spinor; in addition, all nucleon fields include Pauli spinors describing the isospin of the nucleon.

At dimension two, the relativistic πN Lagrangian reads

$$
\mathcal{L}^{(2)}_{\pi N} = \sum_{i=1}^{4} c_i \bar{\Psi} O_i^{(2)} \Psi\,. \quad (34)
$$

The various operators $O_i^{(2)}$ are given in Ref. [36]. The fundamental rule by which this Lagrangian—as well as all the other ones—are assembled is that

they must contain *all* terms consistent with chiral symmetry and Lorentz invariance (apart from other trivial symmetries) at a given chiral dimension (here: order two). The parameters c_i are known as low-energy constants (LECs) and are determined empirically from fits to πN data.

The HB projected πN Lagrangian at order two is most conveniently broken up into two pieces,

$$\widehat{\mathcal{L}}^{(2)}_{\pi N} \;=\; \widehat{\mathcal{L}}^{(2)}_{\pi N,\,\mathrm{fix}} \;+\; \widehat{\mathcal{L}}^{(2)}_{\pi N,\,\mathrm{ct}}\,, \tag{35}$$

with

$$\widehat{\mathcal{L}}^{(2)}_{\pi N,\,\mathrm{fix}} = \bar{N}\left[\frac{1}{2M_N}\,\vec{D}\cdot\vec{D} + i\,\frac{g_A}{4M_N}\,\{\vec{\sigma}\cdot\vec{D}, u_0\}\right] N \tag{36}$$

and

$$\begin{aligned}\widehat{\mathcal{L}}^{(2)}_{\pi N,\,\mathrm{ct}} \;&=\; \bar{N}\left[2\,c_1\,m_\pi^2\,(U+U^\dagger) \;+\; \left(c_2 - \frac{g_A^2}{8M_N}\right) u_0^2 \;+\; c_3\,u_\mu u^\mu \right.\\ &\quad\left. + \frac{i}{2}\left(c_4 + \frac{1}{4M_N}\right)\vec{\sigma}\cdot(\vec{u}\times\vec{u})\right] N\,.\end{aligned} \tag{37}$$

Note that $\widehat{\mathcal{L}}^{(2)}_{\pi N,\,\mathrm{fix}}$ is created entirely from the HB expansion of the relativistic $\mathcal{L}^{(1)}_{\pi N}$ and thus has no free parameters ("fixed"), while $\widehat{\mathcal{L}}^{(2)}_{\pi N,\,\mathrm{ct}}$ is dominated by the new πN contact terms proportional to the c_i parameters, besides some small $1/M_N$ corrections.

At dimension three, the relativistic πN Lagrangian can be formally written as

$$\mathcal{L}^{(3)}_{\pi N} = \sum_{i=1}^{23} d_i \bar{\Psi} O_i^{(3)} \Psi\,, \tag{38}$$

with the operators, $O_i^{(3)}$, listed in Refs. [36, 37]; not all 23 terms are of interest here. The new LECs that occur at this order are the d_i. Similar to the order two case, the HB projected Lagrangian at order three can be broken into two pieces,

$$\widehat{\mathcal{L}}^{(3)}_{\pi N} \;=\; \widehat{\mathcal{L}}^{(3)}_{\pi N,\,\mathrm{fix}} \;+\; \widehat{\mathcal{L}}^{(3)}_{\pi N,\,\mathrm{ct}}\,, \tag{39}$$

with $\widehat{\mathcal{L}}^{(3)}_{\pi N,\,\mathrm{fix}}$ and $\widehat{\mathcal{L}}^{(3)}_{\pi N,\,\mathrm{ct}}$ given in Refs. [36, 37].

3.3 Nucleon Contact Lagrangians

Nucleon contact interactions consist of four nucleon fields (four nucleon legs) and no meson fields. Such terms are needed to renormalize loop integrals,

to make results reasonably independent of regulators, and to parametrize the unresolved short-distance contributions to the nuclear force. For more about contact terms, see Sec. 5.3.

Because of parity, nucleon contact interactions come only in even numbers of derivatives, thus,

$$\mathcal{L}_{NN} = \mathcal{L}_{NN}^{(0)} + \mathcal{L}_{NN}^{(2)} + \mathcal{L}_{NN}^{(4)} + \ldots \tag{40}$$

The lowest order (or leading order) NN Lagrangian has no derivatives and reads [18]

$$\mathcal{L}_{NN}^{(0)} = -\frac{1}{2} C_S \bar{N} N \bar{N} N - \frac{1}{2} C_T \bar{N} \vec{\sigma} N \bar{N} \vec{\sigma} N \,, \tag{41}$$

where N is the heavy baryon nucleon field. C_S and C_T are unknown constants which are determined by a fit to the NN data. The second order NN Lagrangian is given by [19]

$$\begin{aligned}
\mathcal{L}_{NN}^{(2)} \;=\; & -C_1'[(\bar{N}\vec{\nabla}N)^2 + (\overline{\vec{\nabla}N}N)^2] - C_2'(\bar{N}\vec{\nabla}N)\cdot(\overline{\vec{\nabla}N}N) \\
& -C_3'\bar{N}N[\bar{N}\vec{\nabla}^2 N + \overline{\vec{\nabla}^2 N}N] \\
& -iC_4'[\bar{N}\vec{\nabla}N\cdot(\overline{\vec{\nabla}N}\times\vec{\sigma}N) + \overline{(\vec{\nabla}N)}N\cdot(\bar{N}\vec{\sigma}\times\vec{\nabla}N)] \\
& -iC_5'\bar{N}N(\overline{\vec{\nabla}N}\cdot\vec{\sigma}\times\vec{\nabla}N) - iC_6'(\bar{N}\vec{\sigma}N)\cdot(\overline{\vec{\nabla}N}\times\vec{\nabla}N) \\
& -(C_7'\delta_{ik}\delta_{jl} + C_8'\delta_{il}\delta_{kj} + C_9'\delta_{ij}\delta_{kl}) \\
& \times[\bar{N}\sigma_k\partial_i N\bar{N}\sigma_l\partial_j N + \overline{\partial_i N}\sigma_k N\overline{\partial_j N}\sigma_l N] \\
& -(C_{10}'\delta_{ik}\delta_{jl} + C_{11}'\delta_{il}\delta_{kj} + C_{12}'\delta_{ij}\delta_{kl})\bar{N}\sigma_k\partial_i N\overline{\partial_j N}\sigma_l N \\
& -(\frac{1}{2}C_{13}'(\delta_{ik}\delta_{jl} + \delta_{il}\delta_{kj}) \\
& +C_{14}'\delta_{ij}\delta_{kl})[\overline{\partial_i N}\sigma_k\partial_j N + \overline{\partial_j N}\sigma_k\partial_i N]\bar{N}\sigma_l N \,.
\end{aligned} \tag{42}$$

Similar to C_S and C_T, the C_i' are unknown constants which are fixed in a fit to the NN data. Obviously, these contact Lagrangians blow up quite a bit with increasing order, which why we do not give $\mathcal{L}_{NN}^{(4)}$ explicitly here.

4 Nuclear Forces from EFT: Overview

In the beginning of Sec. 3, we spelled out the steps we have to take to accomplish our EFT program for the derivation of nuclear forces. So far, we discussed steps one to three. What is left are steps four (low-momentum expansion) and five (Feynman diagrams). In this section, we will say more about the expansion we are using and give an overview of the Feynman diagrams that arise order by order.

4.1 Chiral Perturbation Theory and Power Counting

In ChPT, we analyze contributions in terms of powers of small momenta over the large scale: $(Q/\Lambda_\chi)^\nu$, where Q stands for a momentum (nucleon three-momentum or pion four-momentum) or a pion mass and $\Lambda_\chi \approx 1$ GeV is the chiral symmetry breaking scale (hadronic scale). Determining the power ν at which a given diagram contributes has become known as power counting. For a non-iterative contribution involving A nucleons, the power ν is given by

$$\nu = -2 + 2A - 2C + 2L + \sum_i \Delta_i \,, \tag{43}$$

with

$$\Delta_i \equiv d_i + \frac{n_i}{2} - 2 \,, \tag{44}$$

where C denotes the number of separately connected pieces and L the number of loops in the diagram; d_i is the number of derivatives or pion-mass insertions and n_i the number of nucleon fields involved in vertex i; the sum runs over all vertices contained in the diagram under consideration. Note that for an irreducible NN diagram ($A = 2$), the above formula reduces to

$$\nu = 2L + \sum_i \Delta_i \tag{45}$$

The power ν is bounded from below; e.g., for $A = 2$, $\nu \geq 0$. This fact is crucial for the power expansion to be of any use.

4.2 The Hierarchy of Nuclear Forces

Chiral perturbation theory and power counting imply that nuclear forces emerge as a hierarchy ruled by the power ν, Fig. 1.

The NN amplitude is determined by two classes of contributions: contact terms and pion-exchange diagrams. There are two contacts of order Q^0 [$\mathcal{O}(Q^0)$] represented by the four-nucleon graph with a small-dot vertex shown in the first row of Fig. 1. The corresponding graph in the second row, four nucleon legs and a solid square, represents the seven contact terms of $\mathcal{O}(Q^2)$. Finally, at $\mathcal{O}(Q^4)$, we have 15 contact contributions represented by a four-nucleon graph with a solid diamond.

Now, turning to the pion contributions: At leading order [LO, $\mathcal{O}(Q^0)$, $\nu = 0$], there is only the well-known static one-pion exchange (1PE), second diagram in the first row of Fig. 1. Two-pion exchange (2PE) starts at next-to-leading order (NLO, $\nu = 2$) and all diagrams of this leading-order two-pion exchange are shown. Further 2PE contributions occur in any higher

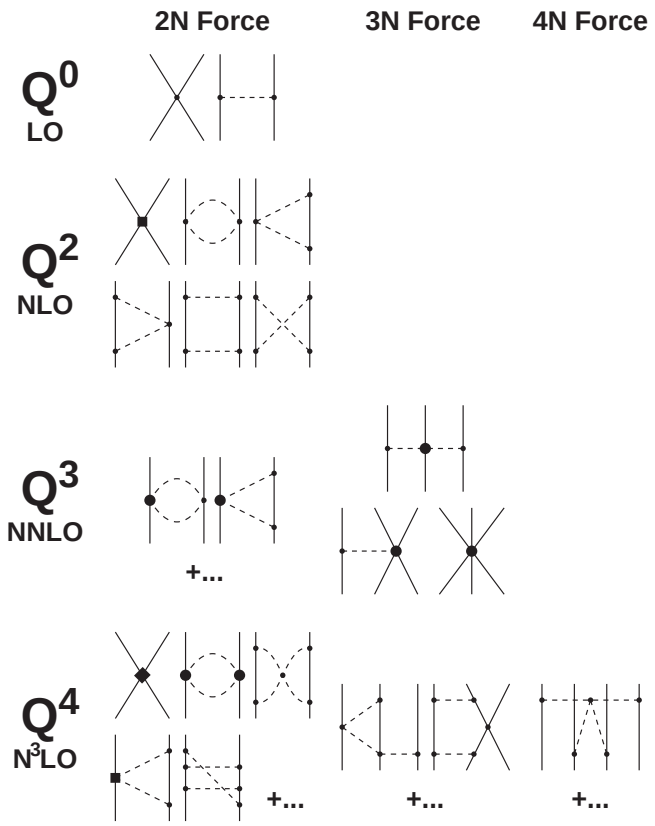

Figure 1: Hierarchy of nuclear forces in ChPT. Solid lines represent nucleons and dashed lines pions. Further explanations are given in the text.

order. Of this sub-leading 2PE, we show only two representative diagrams at next-to-next-to-leading order (NNLO) and three diagrams at next-to-next-to-next-to-leading order (N^3LO).

Finally, there is also three-pion exchange, which shows up for the first time at N^3LO (two loops; one representative 3π diagram is included in Fig. 1). At this order, the 3π contribution is negligible [38].

One important advantage of ChPT is that it makes specific predictions also for many-body forces. For a given order of ChPT, two-nucleon forces (2NF), three-nucleon forces (3NF), ... are generated on the same footing (cf. Fig. 1). At LO, there are no 3NF, and at NLO, all 3NF terms cancel [18, 39]. However, at NNLO and higher orders, well-defined, nonvanishing 3NF

occur [39, 40]. Since 3NF show up for the first time at NNLO, they are weak. Four-nucleon forces (4NF) occur first at N^{3}LO and, therefore, they are even weaker.

5 Two-Nucleon Forces

In this section, we will elaborate in detail on the two-nucleon force contributions of which we have given a rough overview in the previous section.

5.1 Pion-Exchange Contributions in ChPT

The effective pion Lagrangians presented in Sec. 3.2 are the crucial ingredients for the evaluation of the pion-exchange contributions to the NN interaction. We will derive these contributions now order by order.

We will state our results in terms of contributions to the momentum-space NN amplitude in the center-of-mass system (CMS), which takes the general form

$$\begin{aligned} V(\vec{p}\,',\vec{p}) &= V_C + \boldsymbol{\tau}_1\cdot\boldsymbol{\tau}_2\, W_C \\ &+ [\, V_S + \boldsymbol{\tau}_1\cdot\boldsymbol{\tau}_2\, W_S \,]\; \vec{\sigma}_1\cdot\vec{\sigma}_2 \\ &+ [\, V_{LS} + \boldsymbol{\tau}_1\cdot\boldsymbol{\tau}_2\, W_{LS}]\, \Big(-i\vec{S}\cdot(\vec{q}\times\vec{k})\Big) \\ &+ [\, V_T + \boldsymbol{\tau}_1\cdot\boldsymbol{\tau}_2\, W_T \,]\; \vec{\sigma}_1\cdot\vec{q}\;\vec{\sigma}_2\cdot\vec{q} \\ &+ [\, V_{\sigma L} + \boldsymbol{\tau}_1\cdot\boldsymbol{\tau}_2\, W_{\sigma L}\,]\; \vec{\sigma}_1\cdot(\vec{q}\times\vec{k}\,)\; \vec{\sigma}_2\cdot(\vec{q}\times\vec{k}\,)\,, \end{aligned} \tag{46}$$

where $\vec{p}\,'$ and $\vec{p}$ denote the final and initial nucleon momenta in the CMS, respectively; moreover,

$$\begin{aligned} \vec{q} &\equiv \vec{p}\,' - \vec{p} && \text{is the momentum transfer,} \\ \vec{k} &\equiv \tfrac{1}{2}(\vec{p}\,' + \vec{p}) && \text{the average momentum,} \\ \vec{S} &\equiv \tfrac{1}{2}(\vec{\sigma}_1 + \vec{\sigma}_2) && \text{the total spin,} \end{aligned} \tag{47}$$

and $\vec{\sigma}_{1,2}$ and $\boldsymbol{\tau}_{1,2}$ are the spin and isospin operators, respectively, of nucleon 1 and 2. For on-energy-shell scattering, V_α and W_α ($\alpha = C, S, LS, T, \sigma L$) can be expressed as functions of q and k (with $q \equiv |\vec{q}|$ and $k \equiv |\vec{k}|$), only.

Our formalism is similar to the one used by the Munich group [22, 41, 42] except for two differences: all our momentum space amplitudes differ by an over-all factor of (-1) and our spin-orbit potentials, V_{LS} and W_{LS}, differ by an additional factor of (-2). Our conventions are more in tune with what is commonly used in nuclear physics.

In all expressions given below, we will state only the *nonpolynomial* contributions to the NN amplitude. Note, however, that dimensional regularization typically generates also polynomial terms. These polynomials are absorbed by the contact interactions to be discussed in a later section and, therefore, they are of no interest here.

5.1.1 Zeroth Order (LO)

At order zero [$\nu = 0$, $\mathcal{O}(Q^0)$, lowest order, leading order, LO], there is only the well-known static one-pion exchange, second diagram in the first row of Fig. 1 which is given by:

$$V_{1\pi}(\vec{p}\,', \vec{p}) = -\frac{g_A^2}{4f_\pi^2}\, \boldsymbol{\tau}_1 \cdot \boldsymbol{\tau}_2\, \frac{\vec{\sigma}_1 \cdot \vec{q}\, \vec{\sigma}_2 \cdot \vec{q}}{q^2 + m_\pi^2}\,. \tag{48}$$

At first order [$\nu = 1$, $\mathcal{O}(Q)$], there are no pion-exchange contributions (and also no contact terms).

5.1.2 Second Order (NLO)

Non-vanishing higher-order graphs start at second order ($\nu = 2$, next-to-leading order, NLO). The most efficient way to evaluate these loop diagrams is to use covariant perturbation theory and dimensional regularization. This is the method applied by the Munich group [22, 41, 42]. One starts with the relativistic versions of the πN Lagrangians (cf. Sec. 3.2) and sets up four-dimensional (covariant) loop integrals. Relativistic vertices and nucleon propagators are then expanded in powers of $1/M_N$. The divergences that occur in conjunction with the four-dimensional loop integrals are treated by means of dimensional regularization, a prescription which is consistent with chiral symmetry and power counting. The results derived in this way are the same obtained when starting right away with the HB versions of the πN Lagrangians. However, as it turns out, the method used by the Munich group is more efficient in dealing with the rather tedious calculations.

Two-pion exchange occurs first at second order, also know as leading-order 2π exchange. The graphs are shown in the first row of Fig. 2. Since a loop creates already $\nu = 2$, the vertices involved at this order can only be from the leading/lowest order Lagrangian $\widehat{\mathcal{L}}_{\pi N}^{(1)}$, Eq. (33), i. e., they carry only one derivative. These vertices are denoted by small dots in Fig. 2. Concerning the box diagram, we should note that we include only the non-iterative part of this diagram which is obtained by subtracting the iterated 1PE contribution Eq. (65) or Eq. (66), below, but using $M_N^2/E_p \approx$

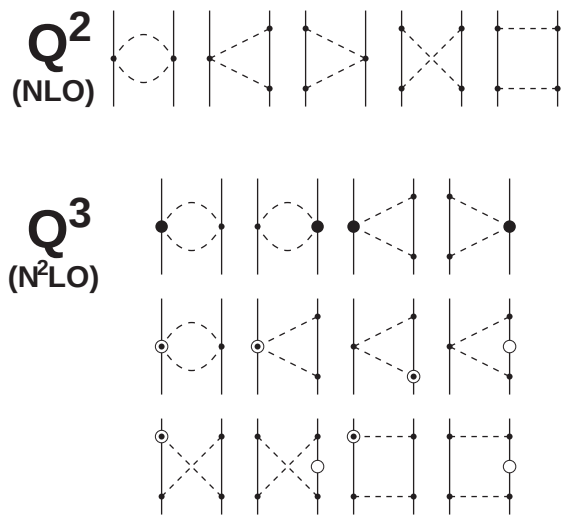

Figure 2: Two-pion exchange contributions to the NN interaction at order two and three in small momenta. Solid lines represent nucleons and dashed lines pions. Small dots denote vertices from the leading order πN Lagrangian $\widehat{\mathcal{L}}^{(1)}_{\pi N}$, Eq. (33). Large solid dots are vertices proportional to the LECs c_i from the second order Lagrangian $\widehat{\mathcal{L}}^{(2)}_{\pi N,\,\mathrm{ct}}$, Eq. (37). Symbols with an open circles are relativistic $1/M_N$ corrections contained in the second order Lagrangian $\widehat{\mathcal{L}}^{(2)}_{\pi N}$, Eqs. (35). Only a few representative examples of $1/M_N$ corrections are shown and not all.

$M_N^2/E_{p''} \approx M_N$ at this order (NLO). Summarizing all contributions from irreducible two-pion exchange at second order, one obtains [22]:

$$\begin{aligned} W_C &= -\frac{L(q)}{384\pi^2 f_\pi^4}\Big[4m_\pi^2(5g_A^4-4g_A^2-1)+q^2(23g_A^4-10g_A^2-1) \\ &\quad +\frac{48g_A^4 m_\pi^4}{w^2}\Big]\,, \qquad (49) \\ V_T &= -\frac{1}{q^2}V_S \;=\; -\frac{3g_A^4 L(q)}{64\pi^2 f_\pi^4}\,, \qquad (50) \end{aligned}$$

where

$$L(q) \equiv \frac{w}{q}\ln\frac{w+q}{2m_\pi} \qquad (51)$$

and

$$w \equiv \sqrt{4m_\pi^2+q^2}\,. \qquad (52)$$

5.1.3 Third Order (NNLO)

The two-pion exchange diagrams of order three ($\nu = 3$, next-to-next-to-leading order, NNLO) are very similar to the ones of order two, except that they contain one insertion from $\widehat{\mathcal{L}}^{(2)}_{\pi N}$, Eq. (35). The resulting contributions are typically either proportional to one of the low-energy constants c_i or they contain a factor $1/M_N$. Notice that relativistic $1/M_N$ corrections can occur for vertices and nucleon propagators. In Fig. 2, we show in row 2 the diagrams with vertices proportional to c_i (large solid dot), Eq. (37), and in row 3 and 4 a few representative graphs with a $1/M_N$ correction (symbols with an open circle). The number of $1/M_N$ correction graphs is large and not all are shown in the figure. Again, the box diagram is corrected for a contribution from the iterated 1PE. If the iterative 2PE of Eq. (65) is used, the expansion of the factor $M_N^2/E_p = M_N - p^2/2M_N + \ldots$ is applied and the term proportional to $(-p^2/2M_N)$ is subtracted from the third order box diagram contribution. Then, one obtains for the full third order contribution [22]:

$$
\begin{aligned}
V_C &= \frac{3g_A^2}{16\pi f_\pi^4}\left\{\frac{g_A^2 m_\pi^5}{16M_N w^2} - \left[2m_\pi^2(2c_1 - c_3) - q^2\left(c_3 + \frac{3g_A^2}{16M_N}\right)\right]\right. \\
&\quad \left.\times\, \widetilde{w}^2 A(q)\right\}\,, \qquad (53)\\
W_C &= \frac{g_A^2}{128\pi M_N f_\pi^4}\left\{3g_A^2 m_\pi^5 w^{-2}\right. \\
&\quad \left. - \left[4m_\pi^2 + 2q^2 - g_A^2(4m_\pi^2 + 3q^2)\right]\widetilde{w}^2 A(q)\right\}\,, \qquad (54)\\
V_T &= -\frac{1}{q^2}V_S \;=\; \frac{9g_A^4\widetilde{w}^2 A(q)}{512\pi M_N f_\pi^4}\,, \qquad (55)\\
W_T &= -\frac{1}{q^2}W_S \\
&= -\frac{g_A^2 A(q)}{32\pi f_\pi^4}\left[\left(c_4 + \frac{1}{4M_N}\right)w^2 - \frac{g_A^2}{8M_N}(10m_\pi^2 + 3q^2)\right]\,, \qquad (56)\\
V_{LS} &= \frac{3g_A^4\widetilde{w}^2 A(q)}{32\pi M_N f_\pi^4}\,, \qquad (57)\\
W_{LS} &= \frac{g_A^2(1-g_A^2)}{32\pi M_N f_\pi^4}w^2 A(q)\,, \qquad (58)
\end{aligned}
$$

with

$$
A(q) \equiv \frac{1}{2q}\arctan\frac{q}{2m_\pi} \qquad (59)
$$

and

$$\widetilde{w} \equiv \sqrt{2m_\pi^2 + q^2}\,. \tag{60}$$

As discussed in Sec. 5.1.5, below, we prefer the iterative 2PE defined in Eq. (66), which leads to a different NNLO term for the iterative 2PE. This changes the $1/M_N$ terms in the above potentials. The changes are obtained by adding to Eqs. (53)-(56) the following terms:

$$V_C = -\frac{3g_A^4}{256\pi f_\pi^4 M_N}(m_\pi\omega^2 + \tilde{\omega}^4 A(q)) \tag{61}$$

$$W_C = \frac{g_A^4}{128\pi f_\pi^4 M_N}(m_\pi\omega^2 + \tilde{\omega}^4 A(q)) \tag{62}$$

$$V_T = -\frac{1}{q^2}V_S = \frac{3g_A^4}{512\pi f_\pi^4 M_N}(m_\pi + \omega^2 A(q)) \tag{63}$$

$$W_T = -\frac{1}{q^2}W_S = -\frac{g_A^4}{256\pi f_\pi^4 M_N}(m_\pi + \omega^2 A(q)) \tag{64}$$

5.1.4 Fourth Order (N^{3}LO)

This order, which may also be denoted by next-to-next-to-next-to-leading order (N^{3}LO), is very involved. Three-pion exchange (3PE) occurs for the first time at this order. The 3PE contribution at N^{3}LO has been calculated by the Munich group and found to be negligible [38]. Therefore, we will ignore it.

The 2PE contributions at N^{3}LO can be subdivided into two groups, one-loop graphs, Fig. 3, and two-loop diagrams, Fig. 4. Since these contributions are very complicated, we have moved them to Appendix A.

5.1.5 Iterated One-Pion-Exchange

Besides all the irreducible 2PE contributions presented above, there is also the reducible 2PE which is generated from iterated 1PE. This "iterative 2PE" is the only 2PE contribution which produces an imaginary part. Thus, one wishes to formulate this contribution such that relativistic elastic unitarity is satisfied. There are several ways to achieve this.

Kaiser *et al.* [22] define the iterative 2PE contribution as follows,

$$V_{2\pi,it}^{(\mathrm{KBW})}(\vec{p}\,',\vec{p}) = \frac{M_N^2}{E_p}\int \frac{d^3p''}{(2\pi)^3}\,\frac{V_{1\pi}(\vec{p}\,',\vec{p}\,'')\,V_{1\pi}(\vec{p}\,'',\vec{p})}{p^2 - p''^2 + i\epsilon} \tag{65}$$

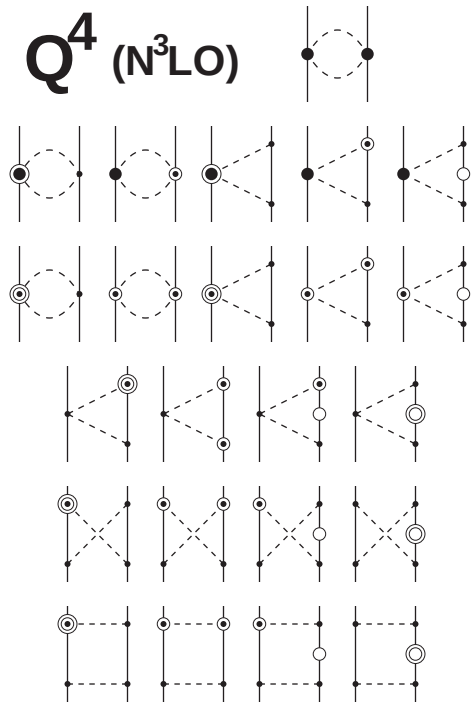

Figure 3: One-loop 2π-exchange contributions to the NN interaction at order four. Basic notation as in Fig. 2. Symbols with a large solid dot and an open circle denote $1/M_N$ corrections of vertices proportional to c_i. Symbols with two open circles mark relativistic $1/M_N^2$ corrections. Both corrections are part of the third order Lagrangian $\widehat{\mathcal{L}}^{(3)}_{\pi N}$, Eq. (39). Representative examples for all types of one-loop graphs that occur at this order are shown.

with $V_{1\pi}$ given in Eq. (48).

Since we adopt the relativistic scheme developed by Blankenbecler and Sugar [43] (BbS) (see beginning of Sec. 5.4), we prefer the following formulation which is consistent with the BbS approach (and, of course, with relativistic elastic unitarity):

$$V^{(\mathrm{EM})}_{2\pi,it}(\vec{p}\,',\vec{p}) = \int \frac{d^3p''}{(2\pi)^3}\,\frac{M_N^2}{E_{p''}}\,\frac{V_{1\pi}(\vec{p}\,',\vec{p}\,'')\,V_{1\pi}(\vec{p}\,'',\vec{p})}{p^2-p''^2+i\epsilon}\,. \tag{66}$$

The iterative 2PE contribution has to be subtracted from the covariant box diagram, order by order. For this, the expansion $M_N^2/E_p = M_N - p^2/2M_N + \ldots$ is applied in Eq. (65) and $M_N^2/E_{p''} = M_N - p''^2/2M_N + \ldots$ in Eq. (66). At NLO, both choices for the iterative 2PE collapse to the same,

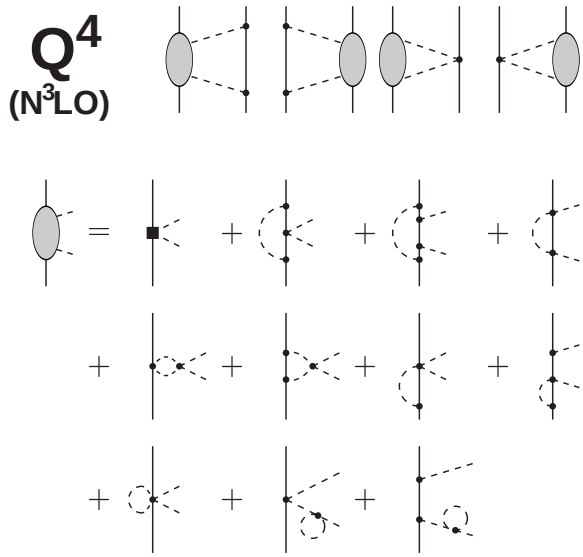

Figure 4: Two-loop 2π-exchange contributions at order four. Basic notation as in Fig. 2. The oval stands for all one-loop πN graphs some of which are shown in the lower part of the figure. The solid square represents vertices proportional to the LECs d_i which are introduced by the third order Lagrangian $\mathcal{L}^{(3)}_{\pi N}$, Eq. (38). More explanations are given in the text.

while at NNLO there are obvious differences.

5.2 NN Scattering in Peripheral Partial Waves Using the Perturbative Amplitude

After the tedious mathematics of the previous section, it is time for more tangible affairs. The obvious question to address now is: How does the derived NN amplitude compare to empirical information? Since our derivation includes only one- and two-pion exchanges, we are dealing here with the long- and intermediate-range part of the NN interaction. This part of the nuclear force is probed in the peripheral partial waves of NN scattering. Thus, in this section, we will calculate the phase shifts that result from the NN amplitudes presented in the previous section and compare them to the empirical phase shifts as well as to the predictions from conventional meson theory. Besides the irreducible two-pion exchanges derived above, we must also include 1PE and iterated 1PE.

In this section [44], which is restricted to just peripheral waves, we

will always consider neutron-proton (np) scattering and take the charge-dependence of 1PE due to pion-mass splitting into account, since it is appreciable. With the definition

$$V_{1\pi}(m_\pi) \equiv -\frac{g_A^2}{4f_\pi^2}\,\frac{\vec{\sigma}_1\cdot\vec{q}\,\vec{\sigma}_2\cdot\vec{q}}{q^2+m_\pi^2}\,, \tag{67}$$

the charge-dependent 1PE for np scattering is

$$V_{1\pi}^{(np)}(\vec{p}\,',\vec{p}) = -V_\pi(m_{\pi^0}) + (-1)^{I+1}\,2\,V_\pi(m_{\pi^\pm})\,, \tag{68}$$

where I denotes the isospin of the two-nucleon system. We use $m_{\pi^0} = 134.9766$ MeV, $m_{\pi^\pm} = 139.5702$ MeV [31], and

$$M_N = \frac{2M_pM_n}{M_p+M_n} = 938.9182\ \text{MeV}\,. \tag{69}$$

Also in the iterative 2PE, we apply the charge-dependent 1PE, i.e., in Eq. (66) we replace $V_{1\pi}$ with $V_{1\pi}^{(np)}$.

The perturbative relativistic T-matrix for np scattering in peripheral waves is

$$T(\vec{p}\,',\vec{p}) = V_{1\pi}^{(np)}(\vec{p}\,',\vec{p}) + V_{2\pi,it}^{(\mathrm{EM},np)}(\vec{p}\,',\vec{p}) + V_{2\pi,irr}(\vec{p}\,',\vec{p})\,, \tag{70}$$

where $V_{2\pi,irr}$ refers to any or all of the irreducible 2PE contributions presented in Sec. 5.1, depending on the order at which the calculation is conducted. In the calculation of the irreducible 2PE, we use the average pion mass $m_\pi = 138.039$ MeV and, thus, neglect the charge-dependence due to pion-mass splitting. The charge-dependence that emerges from irreducible 2π exchange was investigated in Ref. [45] and found to be negligible for partial waves with $L \geq 3$.

For the T-matrix given in Eq. (70), we calculate phase shifts for partial waves with $L \geq 3$ and $T_{lab} \leq 300$ MeV. At order four in small momenta, partial waves with $L \geq 3$ do not receive any contributions from contact interactions and, thus, the non-polynomial pion contributions uniquely predict the F and higher partial waves. We use $f_\pi = 92.4$ MeV [31] and $g_A = 1.29$. Via the Goldberger-Treiman relation, $g_A = g_{\pi NN}\ f_\pi/M_N$, our value for g_A is consistent with $g_{\pi NN}^2/4\pi = 13.63 \pm 0.20$ which is obtained from πN and NN analysis [46, 47].

The LECs used in this calculation are shown in Table 2, column "NN periph. Fig. 5". Note that many determinations of the LECs, c_i and $\bar{d}_i$, can be found in the literature. The most reliable way to determine the LECs

Table 2: Low-energy constants, LECs, used for a NN potential at N^{3}LO, Sec. 5.4.4, and in the calculation of the peripheral NN phase shifts shown in Fig. 5 (column "NN periph. Fig. 5"). The c_i belong to the dimension-two πN Lagrangian, Eq. (37), and are in units of GeV^{-1}, while the $\bar{d}_i$ are associated with the dimension-three Lagrangian, Eq. (38), and are in units of GeV^{-2}. The column "πN empirical" shows determinations from πN data.

LEC	NN potential at N^{3}LO	NN periph. Fig. 5	πN empirical
c_1	–0.81	–0.81	-0.81 ± 0.15^a
c_2	2.80	3.28	3.28 ± 0.23^b
c_3	–3.20	–3.40	-4.69 ± 1.34^a
c_4	5.40	3.40	3.40 ± 0.04^a
$\bar{d}_1 + \bar{d}_2$	3.06	3.06	3.06 ± 0.21^b
$\bar{d}_3$	–3.27	–3.27	-3.27 ± 0.73^b
$\bar{d}_5$	0.45	0.45	0.45 ± 0.42^b
$\bar{d}_{14} - \bar{d}_{15}$	–5.65	–5.65	-5.65 ± 0.41^b

[a]Table 1, Fit 1 of Ref. [48].
[b]Table 2, Fit 1 of Ref. [37].

from empirical πN information is to extract them from the πN amplitude inside the Mandelstam triangle (unphysical region) which can be constructed with the help of dispersion relations from empirical πN data. This method was used by Büttiker and Meißner [48]. Unfortunately, the values for c_2 and all $\bar{d}_i$ parameters obtained in Ref. [48] carry uncertainties, so large that the values cannot provide any guidance. Therefore, in Table 2, only c_1, c_3, and c_4 are from Ref. [48], while the other LECs are taken from Ref. [37] where the πN amplitude in the physical region was considered. To establish a link between πN and NN, we apply the values from the above determinations in our calculations of the NN peripheral phase shifts. In general, we use the mean values; the only exception is c_3, where we choose a value that is, in terms of magnitude, about one standard deviation below the one from Ref. [48]. With the exception of c_3, phase shift predictions do not depend sensitively on variations of the LECs within the quoted uncertainties.

In Fig. 5, we show the phase-shift predictions for neutron-proton scattering in F waves for laboratory kinetic energies below 300 MeV (for G and H waves, see Ref. [26]). The orders displayed are defined as follows:

- Leading order (LO) is just 1PE, Eq. (68).

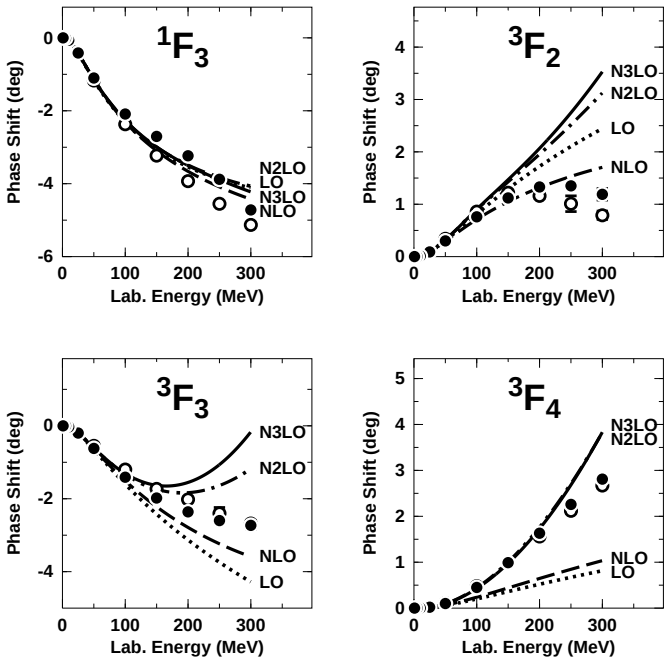

Figure 5: F-wave phase shifts of neutron-proton scattering for laboratory kinetic energies below 300 MeV. We show the predictions from chiral pion exchange at leading order (LO), next-to-leading order (NLO), next-to-next-to-leading order (N2LO), and next-to-next-to-next-to-leading order (N3LO). The solid dots and open circles are the results from the Nijmegen multi-energy np phase shift analysis [49] and the VPI single-energy np analysis SM99 [50], respectively.

- Next-to-leading order (NLO) is 1PE, Eq. (68), plus iterated 1PE, Eq. (66), plus the contributions of Sec. 5.1.2 (order two), Eqs. (49) and (50).
- Next-to-next-to-leading order (denoted by N2LO in the figures) consists of NLO plus the contributions of Sec. 5.1.3 (order three), Eqs. (53)-(58) and (61)-(64).
- Next-to-next-to-next-to-leading order (denoted by N3LO in the figures) consists of N2LO plus the contributions of Sec. 5.1.4 (order four), Eqs. (99)-(112) and (115)-(124).

It is clearly seen in Fig. 5 that the leading order 2π exchange (NLO) is a rather small contribution, insufficient to explain the empirical facts. In

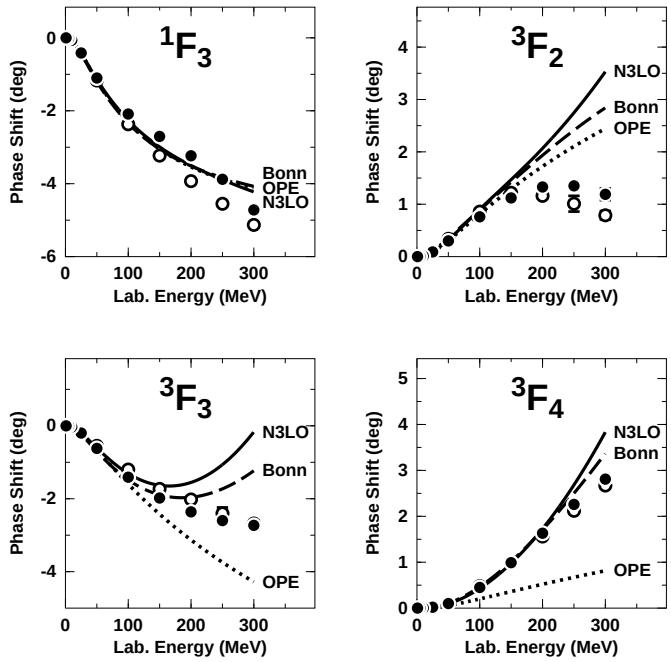

Figure 6: F-wave phase shifts of neutron-proton scattering for laboratory kinetic energies below 300 MeV. We show the results from one-pion-exchange (OPE), and one- plus two-pion exchange as predicted by ChPT at next-to-next-to-next-to-leading order (N3LO) and by the Bonn Full Model [13] (Bonn). Note that the "Bonn" curve does not include the repulsive ω and $\pi\rho$ exchanges of the full model, since this figure serves the purpose to compare just predictions by different models/theories for the $\pi + 2\pi$ contribution to the NN interaction. Empirical phase shifts (solid dots and open circles) as in Fig. 5.

contrast, the next order (N2LO) is very large, several times NLO. This is due to the $\pi\pi NN$ contact interactions proportional to the LECs c_i that are introduced by the second order Lagrangian $\mathcal{L}^{(2)}_{\pi N}$, Eq. (34). These contacts are supposed to simulate the contributions from intermediate Δ-isobars and correlated 2π exchange which are known to be large (see, e. g., Ref. [13]).

At N3LO a clearly identifiable trend towards convergence emerges. Obviously, $^1F_3$ and $^3F_4$ appear fully converged. However, in $^3F_2$ and $^3F_3$, N3LO differs noticeably from NNLO, but the difference is much smaller than the one between NNLO and NLO. This is what we perceive as a trend towards convergence.

In Fig. 6, we conduct a comparison between the predictions from chiral one- and two-pion exchange at N3LO and the corresponding predictions from conventional meson theory (curve 'Bonn'). As representative for conventional meson theory, we choose the Bonn meson-exchange model for the NN interaction [13], since it contains a comprehensive and thoughtfully constructed model for 2π exchange. This 2π model includes box and crossed box diagrams with NN, $N\Delta$, and $\Delta\Delta$ intermediate states as well as direct $\pi\pi$ interaction in S- and P-waves (of the $\pi\pi$ system) consistent with empirical information from πN and $\pi\pi$ scattering. Besides this the Bonn model also includes (repulsive) ω-meson exchange and irreducible diagrams of π and ρ exchange (which are also repulsive). However, note that in the phase shift predictions displayed in Fig. 6, the "Bonn" curve includes only the 1π and 2π contributions from the Bonn model; the short-range contributions are left out since the purpose of the figure is to compare different models/theories for $\pi + 2\pi$. In all waves shown we see, in general, good agreement between N3LO and Bonn. In $^3F_2$ and $^3F_3$ above 150 MeV and in $^3F_4$ above 250 MeV the chiral model at N3LO is more attractive than the Bonn 2π model. Note, however, that the Bonn model is relativistic and, thus, includes relativistic corrections up to infinite orders. Thus, one may speculate that higher orders in ChPT may create some repulsion, moving the Bonn and the chiral predictions even closer together [51].

The 2π exchange contribution to the NN interaction can also be derived from *empirical* πN and $\pi\pi$ input using dispersion theory, which is based upon unitarity, causality (analyticity), and crossing symmetry. The amplitude $N\bar{N} \to \pi\pi$ is constructed from $\pi N \to \pi N$ and $\pi N \to \pi\pi N$ data using crossing properties and analytic continuation; this amplitude is then 'squared' to yield the $N\bar{N}$ amplitude which is related to NN by crossing symmetry [52]. The Paris group [11, 12] pursued this path and calculated NN phase shifts in peripheral partial waves. Naively, the dispersion-theoretic approach is the ideal one, since it is based exclusively on empirical information. Unfortunately, in practice, quite a few uncertainties enter into the approach. First, there are ambiguities in the analytic continuation and, second, the dispersion integrals have to be cut off at a certain momentum to ensure reasonable results. In Ref. [13], a thorough comparison was conducted between the predictions by the Bonn model and the Paris approach and it was demonstrated that the Bonn predictions always lie comfortably within the range of uncertainty of the dispersion-theoretic results. Therefore, there is no need to perform a separate comparison of our chiral N3LO predictions with dispersion theory, since it would not add anything that we cannot conclude from Fig. 6.

Finally, we need to compare the predictions with the empirical phase shifts. In F waves the N^{3}LO predictions above 200 MeV are, in general, too attractive. Note, however, that this is also true for the predictions by the Bonn $\pi + 2\pi$ model. In the *full* Bonn model, besides $\pi + 2\pi$, (repulsive) ω and $\pi\rho$ exchanges are included which move the predictions right on top of the data. The exchange of a ω meson or combined $\pi\rho$ exchange are 3π exchanges. Three-pion exchange occurs first at chiral order four. It has be investigated by Kaiser [38] and found to be negligible, at this order. However, 3π exchange at order five appears to be sizable [53] and may have impact on F waves. Besides this, there is the usual short-range phenomenology. In ChPT, this short-range interaction is parametrized in terms of four-nucleon contact terms (since heavy mesons do not have a place in that theory). Contact terms of order four (N^{3}LO) do not contribute to F-waves, but order six does. In summary, the remaining small discrepancies between the N3LO predictions and the empirical phase shifts may be straightened out in fifth or sixth order of ChPT.

5.3 NN Contact Potentials

In conventional meson theory, the short-range nuclear force is described by the exchange of heavy mesons, notably the $\omega(782)$. The qualitative short-distance behavior of the NN potential is obtained by Fourier transform of the propagator of a heavy meson,

$$\int d^3q \frac{e^{i\vec{q}\cdot\vec{r}}}{m_\omega^2 + \vec{q}^2} \sim \frac{e^{-m_\omega r}}{r} . \tag{71}$$

ChPT is an expansion in small momenta Q, too small to resolve structures like a $\rho(770)$ or $\omega(782)$ meson, because $Q \ll \Lambda_\chi \approx m_{\rho,\omega}$. But the latter relation allows us to expand the propagator of a heavy meson into a power series,

$$\frac{1}{m_\omega^2 + Q^2} \approx \frac{1}{m_\omega^2}\left(1 - \frac{Q^2}{m_\omega^2} + \frac{Q^4}{m_\omega^4} - + \ldots\right), \tag{72}$$

where the ω is representative for any heavy meson of interest. The above expansion suggests that it should be possible to describe the short distance part of the nuclear force simply in terms of powers of Q/m_ω, which fits in well with our over-all power scheme since $Q/m_\omega \approx Q/\Lambda_\chi$.

A second purpose of contact terms is renormalization. Dimensional regularization of the loop integrals of pion-exchanges (cf. Sec. 5.1) typically

generates polynomial terms with coefficients that are, in part, infinite or scale dependent. Contact terms pick up infinities and remove scale dependence.

The partial-wave decomposition of a power Q^ν has an interesting property. First note that Q can only be either the momentum transfer between the two interacting nucleons q or the average momentum k [cf. Eq. (47) for their definitions]. In any case, for even ν,

$$Q^\nu = f_{\frac{\nu}{2}}(\cos\theta)\,, \tag{73}$$

where f_m stands for a polynomial of degree m and θ is the CMS scattering angle. The partial-wave decomposition of Q^ν for a state of orbital-angular momentum L involves the integral

$$I_L^{(\nu)} = \int_{-1}^{+1} Q^\nu P_L(\cos\theta) d\cos\theta = \int_{-1}^{+1} f_{\frac{\nu}{2}}(\cos\theta) P_L(\cos\theta) d\cos\theta\,, \tag{74}$$

where P_L is a Legendre polynomial. Due to the orthogonality of the P_L,

$$I_L^{(\nu)} = 0 \quad \text{for} \quad L > \frac{\nu}{2}\,. \tag{75}$$

Consequently, contact terms of order zero contribute only in S-waves, while order-two terms contribute up to P-waves, order-four terms up to D-waves, etc..

We will now present, one by one, the various orders of NN contact terms together with their partial-wave decomposition [54]. Note that, due to parity, only even powers of Q are allowed.

5.3.1 Zeroth Order

The contact potential at order zero reads:

$$V^{(0)}(\vec{p'}, \vec{p}) = C_S + C_T\, \vec{\sigma}_1 \cdot \vec{\sigma}_2 \tag{76}$$

Partial wave decomposition yields:

$$\begin{aligned} V^{(0)}(^1S_0) &= \widetilde{C}_{^1S_0} = 4\pi\,(C_S - 3\,C_T) \\ V^{(0)}(^3S_1) &= \widetilde{C}_{^3S_1} = 4\pi\,(C_S + C_T) \end{aligned} \tag{77}$$

5.3.2 Second Order

The contact potential contribution of order two is given by:

$$\begin{aligned} V^{(2)}(\vec{p'},\vec{p}) &= C_1 q^2 + C_2 k^2 \\ &+ \left(C_3 q^2 + C_4 k^2\right) \vec{\sigma}_1 \cdot \vec{\sigma}_2 \\ &+ C_5 \left(-i\vec{S} \cdot (\vec{q} \times \vec{k})\right) \\ &+ C_6 (\vec{\sigma}_1 \cdot \vec{q}) (\vec{\sigma}_2 \cdot \vec{q}) \\ &+ C_7 (\vec{\sigma}_1 \cdot \vec{k}) (\vec{\sigma}_2 \cdot \vec{k}) \end{aligned} \tag{78}$$

Second order partial wave contributions:

$$\begin{aligned} V^{(2)}({}^1S_0) &= C_{{}^1S_0}(p^2 + p'^2) \\ &= 4\pi \left(C_1 + \frac{1}{4}C_2 - 3C_3 - \frac{3}{4}C_4 - C_6 - \frac{1}{4}C_7\right)(p^2 + p'^2) \\ V^{(2)}({}^3P_0) &= C_{{}^3P_0}\, pp' \\ &= 4\pi \left(-\frac{2}{3}C_1 + \frac{1}{6}C_2 - \frac{2}{3}C_3 + \frac{1}{6}C_4 - \frac{2}{3}C_5 + 2C_6 - \frac{1}{2}C_7\right) pp' \\ V^{(2)}({}^1P_1) &= C_{{}^1P_1}\, pp' \\ &= 4\pi \left(-\frac{2}{3}C_1 + \frac{1}{6}C_2 + 2C_3 - \frac{1}{2}C_4 + \frac{2}{3}C_6 - \frac{1}{6}C_7\right) pp' \\ V^{(2)}({}^3P_1) &= C_{{}^3P_1}\, pp' \\ &= 4\pi \left(-\frac{2}{3}C_1 + \frac{1}{6}C_2 - \frac{2}{3}C_3 + \frac{1}{6}C_4 - \frac{1}{3}C_5 - \frac{4}{3}C_6 + \frac{1}{3}C_7\right) pp' \\ V^{(2)}({}^3S_1) &= C_{{}^3S_1}(p^2 + p'^2) \\ &= 4\pi \left(C_1 + \frac{1}{4}C_2 + C_3 + \frac{1}{4}C_4 + \frac{1}{3}C_6 + \frac{1}{12}C_7\right)(p^2 + p'^2) \\ V^{(2)}({}^3S_1 - {}^3D_1) &= C_{{}^3S_1 - {}^3D_1} p^2 \\ &= 4\pi \left(-\frac{2\sqrt{2}}{3}C_6 - \frac{2\sqrt{2}}{12}C_7\right) p^2 \\ V^{(2)}({}^3P_2) &= C_{{}^3P_2}\, pp' \\ &= 4\pi \left(-\frac{2}{3}C_1 + \frac{1}{6}C_2 - \frac{2}{3}C_3 + \frac{1}{6}C_4 + \frac{1}{3}C_5\right) pp' \end{aligned} \tag{79}$$

5.3.3 Fourth Order

The contact potential contribution of order four reads:

$$\begin{aligned} V^{(4)}(\vec{p'},\vec{p}) &= D_1 q^4 + D_2 k^4 + D_3 q^2 k^2 + D_4 (\vec{q} \times \vec{k})^2 \\ &+ \left(D_5 q^4 + D_6 k^4 + D_7 q^2 k^2 + D_8 (\vec{q} \times \vec{k})^2\right) \vec{\sigma}_1 \cdot \vec{\sigma}_2 \\ &+ \left(D_9 q^2 + D_{10} k^2\right) \left(-i\vec{S} \cdot (\vec{q} \times \vec{k})\right) \end{aligned}$$

$$
\begin{aligned}
&+ \quad \left(D_{11}q^2 + D_{12}k^2\right)(\vec{\sigma}_1 \cdot \vec{q})\,(\vec{\sigma}_2 \cdot \vec{q}) \\
&+ \quad \left(D_{13}q^2 + D_{14}k^2\right)(\vec{\sigma}_1 \cdot \vec{k})\,(\vec{\sigma}_2 \cdot \vec{k}) \\
&+ \quad D_{15}\left(\vec{\sigma}_1 \cdot (\vec{q} \times \vec{k})\;\vec{\sigma}_2 \cdot (\vec{q} \times \vec{k})\right) \qquad (80)
\end{aligned}
$$

The rather lengthy partial-wave expressions of this order have been relegated to Appendix B.

5.4 Constructing a Chiral NN Potential

5.4.1 Conceptual Questions

The two-nucleon system is non-perturbative as evidenced by the presence of a shallow bound state (the deuteron) and large scattering lengths. Weinberg [18] showed that the strong enhancement of the scattering amplitude arises from purely nucleonic intermediate states. He therefore suggested to use perturbation theory to calculate the NN potential and to apply this potential in a scattering equation to obtain the NN amplitude. We adopt this prescription.

Since the irreducible diagrams that make up the potential are calculated using covariant perturbation theory (cf. Sec. 5.1), it is consistent to start from the covariant Bethe-Salpeter (BS) equation [55] describing two-nucleon scattering. In operator notation, the BS equation reads

$$
T = \mathcal{V} + \mathcal{V}\,\mathcal{G}\,T \qquad (81)
$$

with T the invariant amplitude for the two-nucleon scattering process, $\mathcal{V}$ the sum of all connected two-particle irreducible diagrams, and $\mathcal{G}$ the relativistic two-nucleon propagator. The BS equation is equivalent to a set of two equations

$$
\begin{aligned}
T &= V + V\,g\,T && (82)\\
V &= \mathcal{V} + \mathcal{V}\,(\mathcal{G} - g)\,V && (83)\\
&= \mathcal{V} + \mathcal{V}_{1\pi}\,(\mathcal{G} - g)\,\mathcal{V}_{1\pi} + \ldots\,, && (84)
\end{aligned}
$$

where g is a covariant three-dimensional propagator which preserves relativistic elastic unitarity. We choose the propagator g proposed by Blankenbecler and Sugar (BbS) [43] (for more details on relativistic three-dimensional reductions of the BS equation, see Ref. [7]). The ellipsis in Eq. (84) stands for terms of irreducible 3π and higher pion exchanges which we neglect.

Note that when we speak of covariance in conjunction with (heavy baryon) ChPT, we are not referring to manifest covariance. Relativity and relativistic off-shell effects are accounted for in terms of a Q/M_N expansion up to the given order. Thus, Eq. (84) is evaluated in the following way,

$$V \approx \mathcal{V}(\text{on-shell}) + \mathcal{V}_{1\pi}\,\mathcal{G}\,\mathcal{V}_{1\pi} - V_{1\pi}\,g\,V_{1\pi}\,, \tag{85}$$

where the pion-exchange content of $\mathcal{V}$(on-shell) is $V_{1\pi} + V'_{2\pi}$ with $V_{1\pi}$ the on-shell 1PE given in Eq. (48) and $V'_{2\pi}$ the irreducible 2π exchanges calculated in Sec. 5.1, *but without the box*. $\mathcal{V}_{1\pi}$ denotes the relativistic (off-shell) 1PE. Notice that the term $(\mathcal{V}_{1\pi}\,\mathcal{G}\,\mathcal{V}_{1\pi} - V_{1\pi}\,g\,V_{1\pi})$ represents what has been called "the (irreducible part of the) box diagram contribution" in Sec. 5.1 where it was evaluated at various orders.

The full chiral NN potential V is given by irreducible pion exchanges V_π and contact terms $V_{\rm ct}$,

$$V = V_\pi + V_{\rm ct} \tag{86}$$

with

$$V_\pi = V_{1\pi} + V_{2\pi} + \dots\,, \tag{87}$$

where the ellipsis denotes irreducible 3π and higher pion exchanges which are omitted. Two-pion exchange contributions appear in various orders

$$V_{2\pi} = V_{2\pi}^{(2)} + V_{2\pi}^{(3)} + V_{2\pi}^{(4)} + \dots \tag{88}$$

as calculated in Sec. 5.1. Contact terms come in even orders,

$$V_{\rm ct} = V_{\rm ct}^{(0)} + V_{\rm ct}^{(2)} + V_{\rm ct}^{(4)} + \dots \tag{89}$$

and were presented in Sec. 5.3. The potential V is calculated at a given order. For example, the potential at NNLO includes 2PE up to $V_{2\pi}^{(3)}$ and contacts up to $V_{\rm ct}^{(2)}$. At N^{3}LO, contributions up to $V_{2\pi}^{(4)}$ and $V_{\rm ct}^{(4)}$ are included.

The potential V satisfies the relativistic BbS equation, Eq. (82). Defining

$$\widehat{V}(\vec{p}\,',\vec{p}) \equiv \frac{1}{(2\pi)^3}\sqrt{\frac{M_N}{E_{p'}}}\,V(\vec{p}\,',\vec{p})\,\sqrt{\frac{M_N}{E_p}} \tag{90}$$

and

$$\widehat{T}(\vec{p}\,',\vec{p}) \equiv \frac{1}{(2\pi)^3}\sqrt{\frac{M_N}{E_{p'}}}\,T(\vec{p}\,',\vec{p})\,\sqrt{\frac{M_N}{E_p}} \tag{91}$$

with $E_p \equiv \sqrt{M_N^2 + \vec{p}^2}$ (the factor $1/(2\pi)^3$ is added for convenience), the BbS equation collapses into the usual, nonrelativistic Lippmann-Schwinger (LS) equation,

$$\widehat{T}(\vec{p}\,', \vec{p}) = \widehat{V}(\vec{p}\,', \vec{p}) + \int d^3p''\, \widehat{V}(\vec{p}\,', \vec{p}\,'')\, \frac{M}{p^2 - p''^2 + i\epsilon}\, \widehat{T}(\vec{p}\,'', \vec{p})\,. \qquad (92)$$

Since $\widehat{V}$ satisfies Eq. (92), it can be used like a usual nonrelativistic potential, and $\widehat{T}$ is the conventional nonrelativistic T-matrix.

Iteration of $\widehat{V}$ in the LS equation requires cutting $\widehat{V}$ off for high momenta to avoid infinities, This is consistent with the fact that ChPT is a low-momentum expansion which is valid only for momenta $Q \ll \Lambda_\chi \approx 1$ GeV. Thus, we multiply $\widehat{V}$ with a regulator function

$$\widehat{V}(\vec{p}\,', \vec{p}) \quad \longmapsto \quad \widehat{V}(\vec{p}\,', \vec{p})\, \boldsymbol{e}^{-(p'/\Lambda)^{2n}}\, \boldsymbol{e}^{-(p/\Lambda)^{2n}} \qquad (93)$$

$$\approx \widehat{V}(\vec{p}\,', \vec{p}) \left\{ 1 - \left[\left(\frac{p'}{\Lambda}\right)^{2n} + \left(\frac{p}{\Lambda}\right)^{2n} \right] + \ldots \right\} \qquad (94)$$

with the 'cutoff parameter' Λ around 0.5 GeV. Equation (94) provides an indication of the fact that the exponential cutoff does not necessarily affect the given order at which the calculation is conducted. For sufficiently large n, the regulator introduces contributions that are beyond the given order. Assuming a good rate of convergence of the chiral expansion, such orders are small as compared to the given order and, thus, do not affect the accuracy at the given order. In our calculations we use, of course, the full exponential, Eq. (93), and not the expansion. On a similar note, we also do not expand the square-root factors in Eqs. (90-91) because they are kinematical factors which guarantee relativistic elastic unitarity.

5.4.2 What Order?

Since in nuclear EFT we are dealing with a perturbative expansion, at some point, we have to raise the question, to what order of ChPT we have to go to obtain the precision we need. To discuss this issue on firm grounds, we show in Table 3 the χ^2/datum for the fit of the world np data below 290 MeV for a family of np potentials at NLO and NNLO. The NLO potentials produce the very large χ^2/datum between 67 and 105, and the NNLO are between 12 and 27. The rate of improvement from one order to the other is very encouraging, but the quality of the reproduction of the np data at NLO and NNLO is obviously insufficient for reliable predictions.

Table 3: χ^2/datum for the reproduction of the 1999 *np* database [56] by families of *np* potentials at NLO and NNLO constructed by the Juelich group [57].

$T_{\rm lab}$ bin (MeV)	# of *np* data	— *Juelich np potentials* — NLO	NNLO
0–100	1058	4–5	1.4–1.9
100–190	501	77–121	12–32
190–290	843	140–220	25–69
0–290	2402	67–105	12–27

Based upon these facts, it has been pointed out in 2002 by Entem and Machleidt [25, 26] that one has to proceed to N^{3}LO. Consequently, the first N^{3}LO potential was published in 2003 [27].

At N^{3}LO, there are 24 contact terms (24 parameters) which contribute to the partial waves with $L \leq 2$ (cf. Sec. 5.3). In Table 4, column 'Q^4/N^{3}LO', we show how these terms/parameters are distributed over the various partial waves. For comparison, we also show the number of parameters used in the Nijmegen partial wave analysis (PWA93) [49] and in the high-precision CD-Bonn potential [9]. The table reveals that, for S and P waves, the number of parameters used in high-precision phenomenology and in EFT at N^{3}LO are about the same. Thus, the EFT approach provides retroactively a justification for what the phenomenologists of the 1990's were doing. At NLO and NNLO, the number of parameters is substantially smaller than for PWA93 and CD-Bonn, which explains why these orders are insufficient for a quantitative potential. This fact is also clearly reflected in Fig. 7 where phase shifts are shown for potentials constructed at NLO, NNLO, and N^{3}LO.

5.4.3 Charge-Dependence

For an accurate fit of the low-energy *pp* and *np* data, charge-dependence is important. We include charge-dependence up to next-to-leading order of the isospin-violation scheme (NLØ, in the notation of Ref. [58]). Thus, we include the pion mass difference in 1PE and the Coulomb potential in *pp* scattering, which takes care of the LØ contributions. At order NLØ, we have the pion mass difference in 2PE at NLO, $\pi\gamma$ exchange [59], and two charge-dependent contact interactions of order Q^0 which make possible an accurate fit of the three different $^1S_0$ scattering lengths, a_{pp}, a_{nn}, and a_{np}.

Table 4: Number of parameters needed for fitting the *np* data in phase-shift analysis and by a high-precision NN potential *versus* the number of NN contact terms of EFT based potentials at different orders.

	Nijmegen partial-wave analysis [49]	CD-Bonn high-precision potential [9]	— *Contact Potentials* — Q^0 LO	Q^2 NLO/NNLO	Q^4 N^{3}LO
$^1S_0$	3	4	1	2	4
$^3S_1$	3	4	1	2	4
$^3S_1$-$^3D_1$	2	2	0	1	3
$^1P_1$	3	3	0	1	2
$^3P_0$	3	2	0	1	2
$^3P_1$	2	2	0	1	2
$^3P_2$	3	3	0	1	2
$^3P_2$-$^3F_2$	2	1	0	0	1
$^1D_2$	2	3	0	0	1
$^3D_1$	2	1	0	0	1
$^3D_2$	2	2	0	0	1
$^3D_3$	1	2	0	0	1
$^3D_3$-$^3G_3$	1	0	0	0	0
$^1F_3$	1	1	0	0	0
$^3F_2$	1	2	0	0	0
$^3F_3$	1	2	0	0	0
$^3F_4$	2	1	0	0	0
$^3F_4$-$^3H_4$	0	0	0	0	0
$^1G_4$	1	0	0	0	0
$^3G_3$	0	1	0	0	0
$^3G_4$	0	1	0	0	0
$^3G_5$	0	1	0	0	0
Total	35	38	2	9	24

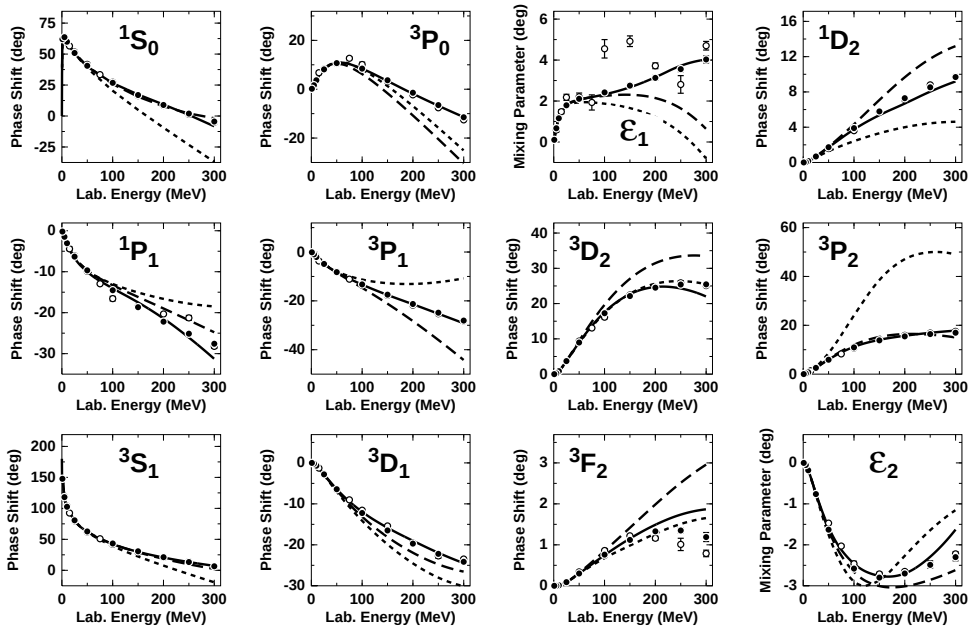

Figure 7: Phase parameters for np scattering as calculated from NN potentials at different orders of ChPT. The dotted line is NLO [57], the dashed NNLO [57], and the solid N^{3}LO [27]. Partial waves with total angular momentum $J \leq 2$ are displayed. Solid dots represent the Nijmegen multienergy np phase shift analysis [49] and open circles are the GWU/VPI single-energy np analysis SM99 [50].

5.4.4 A Quantitative NN Potential at N^{3}LO

NN **Scattering.** The fitting procedure starts with the peripheral partial waves because they depend on fewer parameters. Partial waves with $L \geq 3$ are exclusively determined by 1PE and 2PE because the N^{3}LO contacts contribute to $L \leq 2$ only. 1PE and 2PE at N^{3}LO depend on the axial-vector coupling constant, g_A (we use $g_A = 1.29$), the pion decay constant, $f_\pi = 92.4$ MeV, and eight low-energy constants (LECs) that appear in the dimension-two and dimension-three πN Lagrangians, Eqs. (37) and (38). In the fitting process, we varied three of them, namely, c_2, c_3, and c_4. We found that the other LECs are not very effective in the NN system and, therefore, we kept them at the values determined from πN (cf. Table 2). The most influential constant is c_3, which has to be chosen on the low side (slightly more than one standard deviation below its πN determination) for an optimal fit of the NN data. As compared to a calculation that strictly uses the πN values for c_2 and c_4, our choices for these two LECs lower

Table 5: χ^2/datum for the reproduction of the 1999 ***np* database** [56] by various np potentials. (Numbers in parentheses are the values of cutoff parameters in units of MeV used in the regulators of the chiral potentials.)

$T_{\rm lab}$ bin (MeV)	# of ***np*** data	*Idaho* N^{3}LO [27] (500–600)	*Juelich* N^{3}LO [60] (600/700–450/500)	Argonne V_{18} [61]
0–100	1058	1.0–1.1	1.0–1.1	0.95
100–190	501	1.1–1.2	1.3–1.8	1.10
190–290	843	1.2–1.4	2.8–20.0	1.11
0–290	2402	1.1–1.3	1.7–7.9	1.04

Table 6: χ^2/datum for the reproduction of the 1999 ***pp* database** [56] by various pp potentials. Notation as in Fig. 5.

$T_{\rm lab}$ bin (MeV)	# of ***np*** data	*Idaho* N^{3}LO [27] (500–600)	*Juelich* N^{3}LO [60] (600/700–450/500)	Argonne V_{18} [61]
0–100	795	1.0–1.7	1.0–3.8	1.0
100–190	411	1.5–1.9	3.5–11.6	1.3
190–290	851	1.9–2.7	4.3–44.4	1.8
0–290	2057	1.5–2.1	2.9–22.3	1.4

the $^3F_2$ and $^1F_3$ phase shifts bringing them into closer agreement with the phase shift analysis. The other F waves and the higher partial waves are essentially unaffected by our variations of c_2 and c_4. Overall, the fit of all $J \geq 3$ waves is very good.

We turn now to the lower partial waves. Here, the most important fit parameters are the ones associated with the 24 contact terms that contribute to the partial waves with $L \leq 2$. In addition, we have two charge-dependent contacts which are used to fit the three different $^1S_0$ scattering lengths, a_{pp}, a_{nn}, and a_{np}.

In the optimization procedure, we fit first phase shifts, and then we refine the fit by minimizing the χ^2 obtained from a direct comparison with the data. The χ^2/datum for the fit of the np data below 290 MeV is shown in Table 5, and the corresponding one for pp is given in Table 6. These tables show that at N^{3}LO a χ^2/datum comparable to the high-precision Argonne

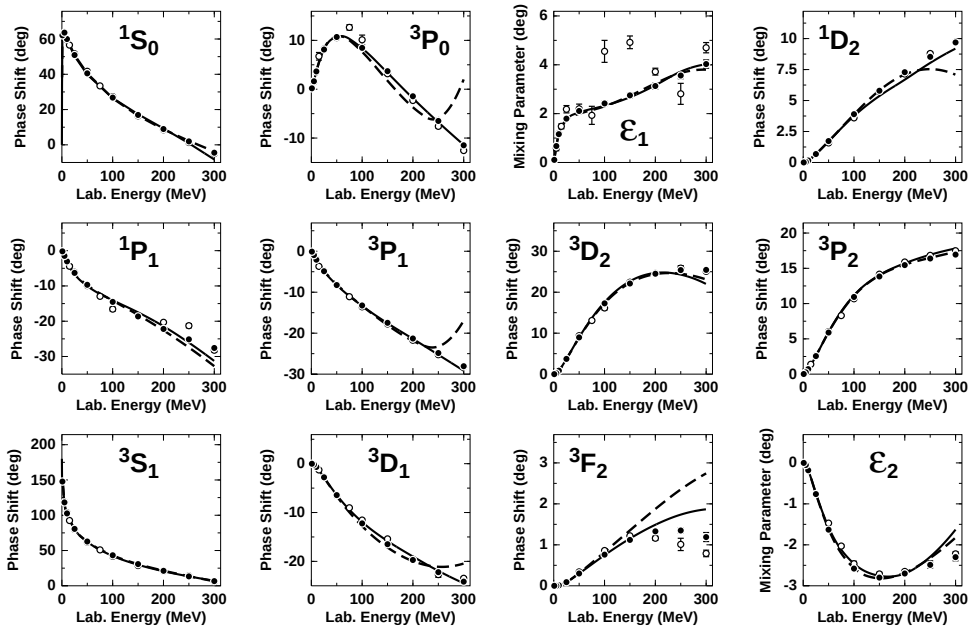

Figure 8: Neutron-proton phase parameters as described by two potentials at N^{3}LO. The solid curve is calculated from the Idaho N^{3}LO potential [27] while the dashed curve is from the Juelich [60] one. Solid dots and open circles as in Fig. 7.

V_{18} [61] potential can, indeed, be achieved. The "Idaho" N^{3}LO potential [27] produces a χ^2/datum = 1.1 for the world *np* data below 290 MeV which compares well with the χ^2/datum = 1.04 by the Argonne potential. In 2005, also the Juelich group produced several N^{3}LO *NN* potentials [60], the best of which fits the *np* data with a χ^2/datum = 1.7 and the worse with a χ^2/datum = 7.9 (see Table 5). While 7.9 is clearly unacceptable for any meaningful application, a χ^2/datum of 1.7 is reasonable, although it does not meet the precision standard that few-nucleon physicists established in the 1990's.

Turning to *pp*, the χ^2 for *pp* data are typically larger than for *np* because of the higher precision of *pp* data. Thus, the Argonne V_{18} produces a χ^2/datum = 1.4 for the world *pp* data below 290 MeV and the best Idaho N^{3}LO *pp* potential obtains 1.5. The fit by the best Juelich N^{3}LO *pp* potential results in a χ^2/datum = 2.9 which, again, is not quite consistent with the precision standards established in the 1990's. The worst Juelich N^{3}LO *pp* potential produces a χ^2/datum of 22.3 and is incompatible with reliable predictions.

Table 7: Deuteron properties as predicted by various NN potentials are compared to empirical information. (Deuteron binding energy B_d, asymptotic S state A_S, asymptotic D/S state η, deuteron radius r_d, quadrupole moment Q, D-state probability P_D; the calculated r_d and Q are without meson-exchange current contributions and relativistic corrections.)

	Idaho N^{3}LO [27] (500)	Juelich N^{3}LO [60] (550/600)	CD-Bonn[9]	AV18[61]	Empirical[a]
B_d (MeV)	2.224575	2.218279	2.224575	2.224575	2.224575(9)
A_S (fm$^{-1/2}$)	0.8843	0.8820	0.8846	0.8850	0.8846(9)
η	0.0256	0.0254	0.0256	0.0250	0.0256(4)
r_d (fm)	1.975	1.977	1.966	1.967	1.97535(85)
Q (fm^2)	0.275	0.266	0.270	0.270	0.2859(3)
P_D (%)	4.51	3.28	4.85	5.76	

[a]See Table XVIII of Ref. [9] for references; the empirical value for r_d is from Ref. [62].

Phase shifts of np scattering from the best Idaho (solid line) and Juelich (dashed line) N^{3}LO np potentials are shown in Figure 8. The phase shifts confirm what the corresponding χ^2 have already revealed.

The Deuteron. The reproduction of the deuteron parameters is shown in Table 7. We present results for two N^{3}LO potentials, namely, Idaho [27] and Juelich [60]. Remarkable are the predictions by the chiral potentials for the deuteron radius which are in good agreement with the latest empirical value obtained by the isotope-shift method [62]. All NN potentials of the past (Table 7 includes two representative examples, namely, CD-Bonn [9] and AV18 [61]) fail to reproduce this very precise new value for the deuteron radius.

In Fig. 9, we display the deuteron wave functions derived from the N^{3}LO potentials and compare them with wave functions based upon conventional NN potentials from the recent past. Characteristic differences are noticeable; in particular, the chiral wave functions are shifted towards larger r which explains the larger deuteron radius.

6 Many-Nucleon Forces

As noted before, an important advantage of the EFT approach to nuclear forces is that it creates two- and many-nucleon forces on an equal footing.

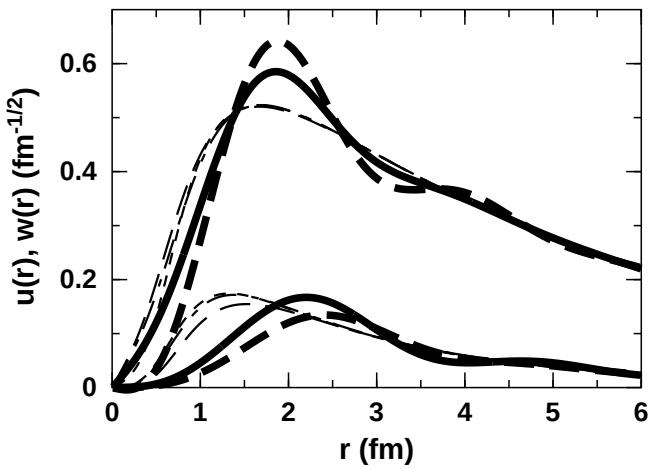

Figure 9: Deuteron wave functions: the family of larger curves are S-waves, the smaller ones D-waves. The thick lines represent the wave functions derived from chiral NN potentials at order N^{3}LO (thick solid: Idaho [27], thick dashed: Juelich [60]). The thin dashed, dash-dotted, and dotted lines refer to the wave functions of the CD-Bonn [9], Nijm-I [8], and AV18 [61] potentials, respectively.

6.1 Three-Nucleon Forces

The first non-vanishing 3NF terms occur at NNLO and are shown in Fig. 10 (cf. also Fig. 1, row 'Q^3/NNLO', column '3N Force'). There are three diagrams: the 2PE, 1PE, and 3N-contact interactions [39, 40]. The 2PE 3N-potential is given by

$$V_{\rm 2PE}^{\rm 3NF} = \left(\frac{g_A}{2f_\pi}\right)^2 \frac{1}{2} \sum_{i\neq j\neq k} \frac{(\vec{\sigma}_i\cdot\vec{q}_i)(\vec{\sigma}_j\cdot\vec{q}_j)}{(q_i^2+m_\pi^2)(q_j^2+m_\pi^2)}\; F_{ijk}^{\alpha\beta}\; \tau_i^\alpha \tau_j^\beta \tag{95}$$

with $\vec{q}_i \equiv \vec{p}_i{}' - \vec{p}_i$, where $\vec{p}_i$ and $\vec{p}_i{}'$ are the initial and final momenta of nucleon i, respectively, and

$$F_{ijk}^{\alpha\beta} = \delta^{\alpha\beta}\left[-\frac{4c_1 m_\pi^2}{f_\pi^2} + \frac{2c_3}{f_\pi^2}\;\vec{q}_i\cdot\vec{q}_j\right] + \frac{c_4}{f_\pi^2}\sum_\gamma \epsilon^{\alpha\beta\gamma}\;\tau_k^\gamma\;\vec{\sigma}_k\cdot[\vec{q}_i\times\vec{q}_j]\;. \tag{96}$$

The vertex involved in this 3NF term is the two-derivative $\pi\pi NN$ vertex (solid square in Fig. 10) which we encountered already in the 2PE contribution to the NN potential at NNLO. Thus, there are no new parameters and

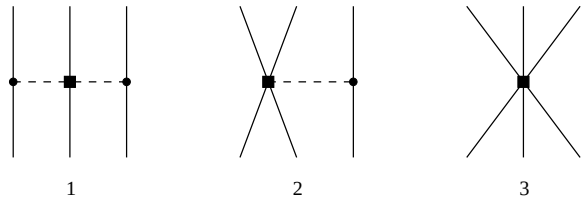

Figure 10: The three-nucleon force at NNLO (from Ref. [40]).

the contribution is fixed by the LECs used in NN. The 1PE contribution is

$$V_{\rm 1PE}^{\rm 3NF} = D\,\frac{g_A}{8f_\pi^2}\sum_{i\neq j\neq k}\frac{\vec{\sigma}_j\cdot\vec{q}_j}{q_j^2+m_\pi^2}(\boldsymbol{\tau}_i\cdot\boldsymbol{\tau}_j)(\vec{\sigma}_i\cdot\vec{q}_j) \tag{97}$$

and, finally, the 3N contact term reads

$$V_{\rm ct}^{\rm 3NF} = E\,\frac{1}{2}\sum_{j\neq k}\boldsymbol{\tau}_j\cdot\boldsymbol{\tau}_k\ . \tag{98}$$

The last two 3NF terms involve two new vertices (that do not appear in the 2N problem), namely, the $\pi NNNN$ vertex with parameter D and a $6N$ vertex with parameters E. To pin them down, one needs two observables that involve at least three nucleons. In Ref. [40], the triton binding energy and the nd doublet scattering length ${}^2a_{nd}$ were used. Alternatively, one may also choose the binding energies of ^{3}H and ^{4}He [63]. Once D and E are fixed, the results for other 3N, 4N, ...observables are predictions. In Refs. [64, 63], the first calculations of the structure of light nuclei (^{6}Li and ^{7}Li) were reported. Recently, the structure of nuclei with $A = 10-13$ nucleons has been calculated using the *ab initio* no-core shell model and applying chiral two and three-nucleon forces [65]. The results are very encouraging. Concerning the famous 'A_y puzzle', the above 3NF terms yield some improvement of the predicted nd A_y, however, the problem is not solved [40].

Note that the 3NF expressions given in Eqs. (95)-(98) above are the ones that occur at NNLO, and all calculations to date have included only those. Since we have to proceed to N^{3}LO for sufficient accuracy of the 2NF, then consistency requires that we also consider the 3NF at N^{3}LO. The 3NF at N^{3}LO is very involved as can be seen from Fig. 11, but it does not depend on any new parameters. It is presently under construction [66]. So, for the moment, we can only hope that the A_y puzzle may be solved by a complete calculation at N^{3}LO.

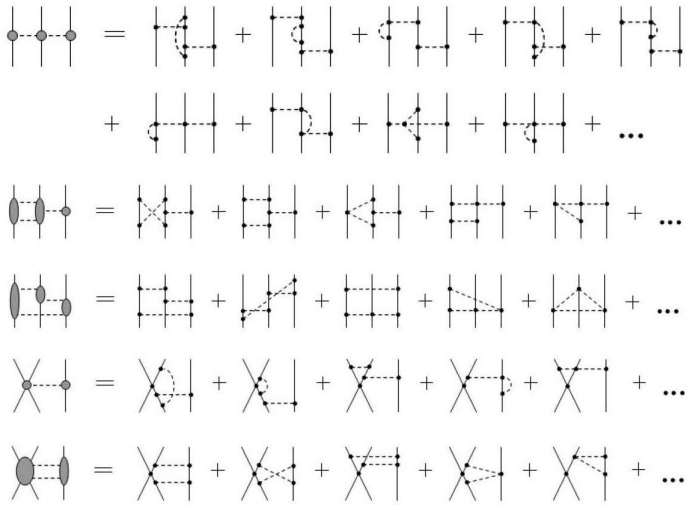

Figure 11: Three-nucleon force contributions at N^{3}LO (from Ref. [66]).

6.2 Four-Nucleon Forces

In ChPT, four-nucleon forces (4NF) appear for the first time at N^{3}LO ($\nu = 4$). Thus, N^{3}LO is the leading order for 4NF. Assuming a good rate of convergence, a contribution of order $(Q/\Lambda_\chi)^4$ is expected to be rather small. Thus, ChPT predicts 4NF to be essentially insignificant, consistent with experience. Still, nothing is fully proven in physics unless we have performed explicit calculations. Very recently, the first such calculation has been performed: The chiral 4NF, Fig. 12, has been applied in a calculation of the ^{4}He binding energy and found to contribute a few 100 keV [68]. It should be noted that this preliminary calculation involves many approximations, but it certainly provides the right order of magnitude of the result, which is indeed very small as compared to the full ^{4}He binding energy of 28.3 MeV.

7 Conclusions

The theory of nuclear forces has made great progress since the turn of the millennium. Nucleon-nucleon potentials have been developed that are based on proper theory (EFT for low-energy QCD) and are of high-precision, at the same time. Moreover, the theory generates two- and many-body forces on an equal footing and provides a theoretical explanation for the empirically known fact that 2NF $\gg$ 3NF $\gg$ 4NF ....

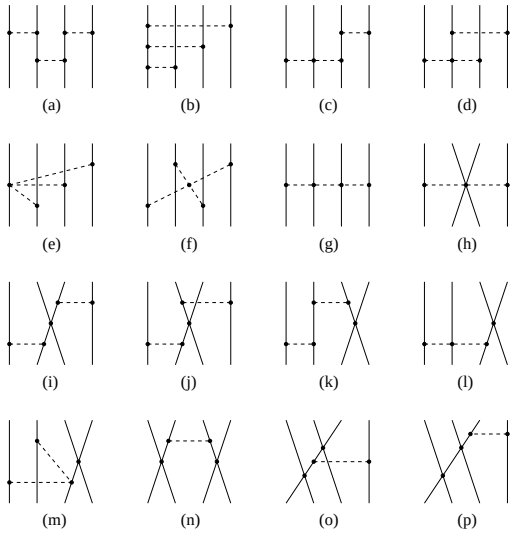

Figure 12: The four-nucleon force at N^{3}LO (from Ref. [67]).

At N^{3}LO [26, 27], the accuracy can be achieved that is necessary and sufficient for reliable microscopic nuclear structure predictions. First calculations applying the N^{3}LO NN potential [27] in the conventional shell model [69, 70], the *ab initio* no-core shell model [71, 72, 73], the coupled cluster formalism [74, 75, 76, 77, 78], and the unitary-model-operator approach [79] have produced promising results.

The 3NF at NNLO is known [39, 40] and has been applied in few-nucleon reactions [40, 80, 81] as well as the structure of light nuclei [64, 63, 65]. However, the famous 'A_y puzzle' of nucleon-deuteron scattering is not resolved by the 3NF at NNLO. Thus, one important outstanding issue is the 3NF at N^{3}LO, which is under construction [66].

Another open question that needs to be settled is whether Weinberg power counting, which is applied in all current NN potentials, is consistent. This controversial issue is presently being debated in the literature [82, 83].

Acknowledgements

It is a pleasure to thank the organizers of this workshop, particularly, Ananda Santra, for their warm hospitality. I gratefully acknowledge numerous discussions with my collaborator D. R. Entem. This work was supported in part by the U.S. National Science Foundation under Grant No. PHY-0099444.

A Fourth Order Two-Pion Exchange Contributions

The fourth order 2PE contributions consist of two classes: the one-loop (Fig. 3) and the two-loop diagrams (Fig. 4).

A.1 One-loop diagrams

This large pool of diagrams can be analyzed in a systematic way by introducing the following well-defined subdivisions.

A.1.1 c_i^2 contributions.

The only contribution of this kind comes from the football diagram with both vertices proportional to c_i (first row of Fig. 3). One obtains [41]:

$$V_C = \frac{3L(q)}{16\pi^2 f_\pi^4}\left[\left(\frac{c_2}{6}w^2 + c_3\widetilde{w}^2 - 4c_1 m_\pi^2\right)^2 + \frac{c_2^2}{45}w^4\right], \tag{99}$$

$$\begin{aligned} W_T &= -\frac{1}{q^2}W_S \\ &= \frac{c_4^2 w^2 L(q)}{96\pi^2 f_\pi^4}. \end{aligned} \tag{100}$$

A.1.2 c_i/M_N contributions.

This class consists of diagrams with one vertex proportional to c_i and one $1/M_N$ correction. A few graphs that are representative for this class are shown in the second row of Fig. 3. Symbols with a large solid dot and an open circle denote $1/M_N$ corrections of vertices proportional to c_i. They are part of $\widehat{\mathcal{L}}_{\pi N}^{(3)}$, Eq. (39). The result for this group of diagrams is [41]:

$$\begin{aligned} V_C &= -\frac{g_A^2 L(q)}{32\pi^2 M_N f_\pi^4}\Big[(c_2 - 6c_3)q^4 + 4(6c_1 + c_2 - 3c_3)q^2 m_\pi^2 \\ &\quad +6(c_2 - 2c_3)m_\pi^4 + 24(2c_1 + c_3)m_\pi^6 w^{-2}\Big], \end{aligned} \tag{101}$$

$$W_C = -\frac{c_4 q^2 L(q)}{192\pi^2 M_N f_\pi^4}\left[g_A^2(8m_\pi^2 + 5q^2) + w^2\right], \tag{102}$$

$$\begin{aligned} W_T &= -\frac{1}{q^2}W_S \\ &= -\frac{c_4 L(q)}{192\pi^2 M_N f_\pi^4}\left[g_A^2(16m_\pi^2 + 7q^2) - w^2\right], \end{aligned} \tag{103}$$

$$V_{LS} = \frac{c_2\, g_A^2}{8\pi^2 M_N f_\pi^4}\, w^2 L(q)\,, \tag{104}$$

$$W_{LS} = -\frac{c_4 L(q)}{48\pi^2 M_N f_\pi^4}\left[g_A^2(8m_\pi^2+5q^2)+w^2\right]\,. \tag{105}$$

A.1.3 $1/M_N^2$ corrections.

These are relativistic $1/M_N^2$ corrections of the leading order 2π exchange diagrams. Typical examples for this large class are shown in row 3–6 of Fig. 3. This time, there is no correction from the iterated 1PE, Eq. (65) or Eq. (66), since the expansion of the factor M_N^2/E_p does not create a term proportional to $1/M_N^2$. The total result for this class is [42],

$$V_C = -\frac{g_A^4}{32\pi^2 M_N^2 f_\pi^4}\left[L(q)\left(2m_\pi^8 w^{-4}+8m_\pi^6 w^{-2}-q^4-2m_\pi^4\right)+\frac{m_\pi^6}{2w^2}\right] \tag{106}$$

$$\begin{aligned} W_C = & -\frac{1}{768\pi^2 M_N^2 f_\pi^4}\Bigg\{L(q)\Bigg[8g_A^2\left(\frac{3}{2}q^4+3m_\pi^2q^2+3m_\pi^4-6m_\pi^6w^{-2}\right.\\ & \left.-k^2(8m_\pi^2+5q^2)\right)+4g_A^4\Big(k^2(20m_\pi^2+7q^2-16m_\pi^4w^{-2})+16m_\pi^8w^{-4}\\ & +12m_\pi^6w^{-2}-4m_\pi^4q^2w^{-2}-5q^4-6m_\pi^2q^2-6m_\pi^4\Big)-4k^2w^2\Bigg]\\ & +\frac{16g_A^4m_\pi^6}{w^2}\Bigg\}\,, \end{aligned} \tag{107}$$

$$V_T = -\frac{1}{q^2}V_S = \frac{g_A^4\, L(q)}{32\pi^2 M_N^2 f_\pi^4}\left(k^2+\frac{5}{8}q^2+m_\pi^4w^{-2}\right), \tag{108}$$

$$\begin{aligned} W_T = & -\frac{1}{q^2}W_S = \frac{L(q)}{1536\pi^2 M_N^2 f_\pi^4}\Bigg[4g_A^4\left(7m_\pi^2+\frac{17}{4}q^2+4m_\pi^4w^{-2}\right)\\ & -32g_A^2\left(m_\pi^2+\frac{7}{16}q^2\right)+w^2\Bigg]\,, \end{aligned} \tag{109}$$

$$V_{LS} = \frac{g_A^4\, L(q)}{4\pi^2 M_N^2 f_\pi^4}\left(\frac{11}{32}q^2+m_\pi^4w^{-2}\right), \tag{110}$$

$$\begin{aligned} W_{LS} = & \frac{L(q)}{256\pi^2 M_N^2 f_\pi^4}\Bigg[16g_A^2\left(m_\pi^2+\frac{3}{8}q^2\right)\\ & +\frac{4}{3}\,g_A^4\left(4m_\pi^4w^{-2}-\frac{11}{4}q^2-9m_\pi^2\right)-w^2\Bigg]\,, \end{aligned} \tag{111}$$

$$V_{\sigma L} = \frac{g_A^4\, L(q)}{32\pi^2 M_N^2 f_\pi^4}\,. \tag{112}$$

A.2 Two-loop contributions.

The two-loop contributions are quite intricate. In Fig. 4, we attempt a graphical representation of this class. The gray disk stands for all one-loop πN graphs which are shown in some detail in the lower part of the figure. Not all of the numerous graphs are displayed. Some of the missing ones are obtained by permutation of the vertices along the nucleon line, others by inverting initial and final states. Vertices denoted by a small dot are from the leading order πN Lagrangian $\widehat{\mathcal{L}}^{(1)}_{\pi N}$, Eq. (33), except for the four-pion vertices which are from $\mathcal{L}^{(2)}_{\pi\pi}$, Eq. (27). The solid square represents vertices proportional to the LECs d_i which are introduced by the third order Lagrangian $\mathcal{L}^{(3)}_{\pi N}$, Eq. (38). The d_i vertices occur actually in one-loop NN diagrams, but we list them among the two-loop NN contributions because they are needed to absorb divergences generated by one-loop πN graphs. Using techniques from dispersion theory, Kaiser [41] calculated the imaginary parts of the NN amplitudes, Im $V_\alpha(i\mu)$ and Im $W_\alpha(i\mu)$, which result from analytic continuation to time-like momentum transfer $q = i\mu - 0^+$ with $\mu \geq 2m_\pi$. From this, the momentum-space amplitudes $V_\alpha(q)$ and $W_\alpha(q)$ are obtained via the subtracted dispersion relations:

$$V_{C,S}(q) = -\frac{2q^6}{\pi}\int_{2m_\pi}^{\infty} d\mu\, \frac{\mathrm{Im}\, V_{C,S}(i\mu)}{\mu^5(\mu^2+q^2)}\,, \tag{113}$$

$$V_T(q) = \frac{2q^4}{\pi}\int_{2m_\pi}^{\infty} d\mu\, \frac{\mathrm{Im}\, V_T(i\mu)}{\mu^3(\mu^2+q^2)}\,, \tag{114}$$

and similarly for $W_{C,S,T}$.

In most cases, the dispersion integrals can be solved analytically and the following expressions are obtained [26]:

$$V_C(q) = \frac{3g_A^4\widetilde{w}^2 A(q)}{1024\pi^2 f_\pi^6}\left[(m_\pi^2+2q^2)\left(2m_\pi+\widetilde{w}^2 A(q)\right)+4g_A^2 m_\pi \widetilde{w}^2\right]; \tag{115}$$

$$W_C(q) = W_C^{(a)}(q) + W_C^{(b)}(q)\,, \tag{116}$$

with

$$W_C^{(a)}(q) = \frac{L(q)}{18432\pi^4 f_\pi^6}\Bigg\{192\pi^2 f_\pi^2 w^2 \bar{d}_3\left[2g_A^2\widetilde{w}^2 - \frac{3}{5}(g_A^2-1)w^2\right]$$

$$
\begin{aligned}
&+\left[6g_A^2\widetilde{w}^2-(g_A^2-1)w^2\right]\Bigg[384\pi^2 f_\pi^2\left(\widetilde{w}^2(\bar{d}_1+\bar{d}_2)+4m_\pi^2\bar{d}_5\right)\\
&+L(q)\left(4m_\pi^2(1+2g_A^2)+q^2(1+5g_A^2)\right)\\
&-\left(\frac{q^2}{3}(5+13g_A^2)+8m_\pi^2(1+2g_A^2)\right)\Bigg]\Bigg\} \qquad (117)
\end{aligned}
$$

and

$$
W_C^{(b)}(q) = -\frac{2q^6}{\pi}\int_{2m_\pi}^{\infty} d\mu\,\frac{\mathrm{Im}\,W_C^{(b)}(i\mu)}{\mu^5(\mu^2+q^2)}\,, \qquad (118)
$$

where

$$
\begin{aligned}
\mathrm{Im}\,W_C^{(b)}(i\mu) &= -\frac{2\kappa}{3\mu(8\pi f_\pi^2)^3}\int_0^1 dx\left[g_A^2(2m_\pi^2-\mu^2)+2(g_A^2-1)\kappa^2x^2\right]\\
&\times\Bigg\{-3\kappa^2x^2+6\kappa x\sqrt{m_\pi^2+\kappa^2x^2}\,\ln\frac{\kappa x+\sqrt{m_\pi^2+\kappa^2x^2}}{m_\pi}\\
&+g_A^4\left(\mu^2-2\kappa^2x^2-2m_\pi^2\right)\Bigg[\frac{5}{6}+\frac{m_\pi^2}{\kappa^2x^2}-\left(1+\frac{m_\pi^2}{\kappa^2x^2}\right)^{3/2}\\
&\times\ln\frac{\kappa x+\sqrt{m_\pi^2+\kappa^2x^2}}{m_\pi}\Bigg]\Bigg\}\,; \qquad (119)
\end{aligned}
$$

$$
\begin{aligned}
V_T(q) &= V_T^{(a)}(q)+V_T^{(b)}(q)\\
&= -\frac{1}{q^2}V_S(q) \;=\; -\frac{1}{q^2}\left(V_S^{(a)}(q)+V_S^{(b)}(q)\right), \qquad (120)
\end{aligned}
$$

with

$$
V_T^{(a)}(q) = -\frac{1}{q^2}V_S^{(a)}(q) \;=\; -\frac{g_A^2w^2L(q)}{32\pi^2f_\pi^4}(\bar{d}_{14}-\bar{d}_{15}) \qquad (121)
$$

and

$$
V_T^{(b)}(q) = -\frac{1}{q^2}V_S^{(b)}(q) \;=\; \frac{2q^4}{\pi}\int_{2m_\pi}^{\infty} d\mu\,\frac{\mathrm{Im}\,V_T^{(b)}(i\mu)}{\mu^3(\mu^2+q^2)}\,, \qquad (122)
$$

where

$$
\begin{aligned}
\mathrm{Im}\,V_T^{(b)}(i\mu) &= -\frac{2g_A^6\kappa^3}{\mu(8\pi f_\pi^2)^3}\int_0^1 dx(1-x^2)\Bigg[-\frac{1}{6}+\frac{m_\pi^2}{\kappa^2x^2}\\
&-\left(1+\frac{m_\pi^2}{\kappa^2x^2}\right)^{3/2}\ln\frac{\kappa x+\sqrt{m_\pi^2+\kappa^2x^2}}{m_\pi}\Bigg]\,; \qquad (123)
\end{aligned}
$$

$$
W_T(q) = -\frac{1}{q^2}W_S(q) = \frac{g_A^4w^2A(q)}{2048\pi^2f_\pi^6}\left[w^2A(q)+2m_\pi(1+2g_A^2)\right], \qquad (124)
$$

where $\kappa \equiv \sqrt{\mu^2/4 - m_\pi^2}$.

Note that the analytic solutions hold modulo polynomials. We have checked the importance of those contributions where we could not find an analytic solution and where, therefore, the integrations have to be performed numerically. It turns out that the combined effect on NN phase shifts from $W_C^{(b)}$, $V_T^{(b)}$, and $V_S^{(b)}$ is smaller than 0.1 deg in F and G waves and smaller than 0.01 deg in H waves, at $T_{\rm lab} = 300$ MeV (and less at lower energies). This renders these contributions negligible. Therefore, we omit $W_C^{(b)}$, $V_T^{(b)}$, and $V_S^{(b)}$ in the construction of chiral NN potentials at order N^{3}LO.

In Eqs. (117) and (121), we use the scale-independent LECs, $\bar{d}_i$, which are obtained by combining the scale-dependent ones, $d_i^r(\lambda)$, with the chiral logarithm, $\ln(m_\pi/\lambda)$, or equivalently $\bar{d}_i = d_i^r(m_\pi)$. The scale-dependent LECs, $d_i^r(\lambda)$, are a consequence of renormalization. For more details about this issue, see Ref. [37].

B Partial Wave Decomposition of the Fourth Order Contact Potential

The contact potential contribution of order four, Eq. (80), decomposes into partial-waves as follows.

$$
\begin{aligned}
V^{(4)}(^1S_0) &= \widehat{D}_{^1S_0}(p'^4 + p^4) + D_{^1S_0} p'^2 p^2 \\
V^{(4)}(^3P_0) &= D_{^3P_0}(p'^3 p + p' p^3) \\
V^{(4)}(^1P_1) &= D_{^1P_1}(p'^3 p + p' p^3) \\
V^{(4)}(^3P_1) &= D_{^3P_1}(p'^3 p + p' p^3) \\
V^{(4)}(^3S_1) &= \widehat{D}_{^3S_1}(p'^4 + p^4) + D_{^3S_1} p'^2 p^2 \\
V^{(4)}(^3D_1) &= D_{^3D_1} p'^2 p^2 \\
V^{(4)}(^3S_1 -^3 D_1) &= \widehat{D}_{^3S_1-^3D_1} p^4 + D_{^3S_1-^3D_1} p'^2 p^2 \\
V^{(4)}(^1D_2) &= D_{^1D_2} p'^2 p^2 \\
V^{(4)}(^3D_2) &= D_{^3D_2} p'^2 p^2 \\
V^{(4)}(^3P_2) &= D_{^3P_2}(p'^3 p + p' p^3) \\
V^{(4)}(^3P_2 -^3 F_2) &= D_{^3P_2-^3F_2} p' p^3 \\
V^{(4)}(^3D_3) &= D_{^3D_3} p'^2 p^2
\end{aligned}
\tag{125}
$$

The coefficients in the above expressions are given by:

$$
\begin{aligned}
\widehat{D}_{1_{S_0}} &= D_1 + \frac{1}{16}D_2 + \frac{1}{4}D_3 - 3D_5 - \frac{3}{16}D_6 - \frac{3}{4}D_7 - D_{11} - \frac{1}{4}D_{12} - \frac{1}{4}D_{13} \\
&\quad -\frac{1}{16}D_{14} \\
D_{1_{S_0}} &= \frac{10}{3}D_1 + \frac{5}{24}D_2 + \frac{1}{6}D_3 + \frac{2}{3}D_4 - 10D_5 - \frac{5}{8}D_6 - \frac{1}{2}D_7 - 2D_8 - \frac{10}{3}D_{11} \\
&\quad -\frac{1}{6}D_{12} - \frac{1}{6}D_{13} - \frac{5}{24}D_{14} - \frac{2}{3}D_{15} \\
D_{3_{P_0}} &= -\frac{4}{3}D_1 + \frac{1}{12}D_2 - \frac{4}{3}D_5 + \frac{1}{12}D_6 - \frac{2}{3}D_9 - \frac{1}{6}D_{10} + \frac{8}{3}D_{11} + \frac{1}{3}D_{12} - \frac{1}{3}D_{13} \\
&\quad -\frac{1}{6}D_{14} \\
D_{1_{P_1}} &= -\frac{4}{3}D_1 + \frac{1}{12}D_2 + 4D_5 - \frac{1}{4}D_6 + \frac{4}{3}D_{11} - \frac{1}{12}D_{14} \\
D_{3_{P_1}} &= -\frac{4}{3}D_1 + \frac{1}{12}D_2 - \frac{4}{3}D_5 + \frac{1}{12}D_6 - \frac{1}{3}D_9 - \frac{1}{12}D_{10} - 2D_{11} - \frac{1}{6}D_{12} + \frac{1}{6}D_{13} \\
&\quad +\frac{1}{8}D_{14} \\
\widehat{D}_{3_{S_1}} &= D_1 + \frac{1}{16}D_2 + \frac{1}{4}D_3 + D_5 + \frac{1}{16}D_6 + \frac{1}{4}D_7 + \frac{1}{3}D_{11} + \frac{1}{12}D_{12} + \frac{1}{12}D_{13} \\
&\quad +\frac{1}{48}D_{14} \\
D_{3_{S_1}} &= \frac{10}{3}D_1 + \frac{5}{24}D_2 + \frac{1}{6}D_3 + \frac{2}{3}D_4 + \frac{10}{3}D_5 + \frac{5}{24}D_6 + \frac{1}{6}D_7 + \frac{2}{3}D_8 + \frac{10}{9}D_{11} \\
&\quad +\frac{1}{18}D_{12} + \frac{1}{18}D_{13} + \frac{5}{72}D_{14} + \frac{2}{9}D_{15} \\
D_{3_{D_1}} &= \frac{8}{15}D_1 + \frac{1}{30}D_2 - \frac{2}{15}D_3 - \frac{2}{15}D_4 + \frac{8}{15}D_5 + \frac{1}{30}D_6 - \frac{2}{15}D_7 - \frac{2}{15}D_8 \\
&\quad +\frac{2}{5}D_9 - \frac{1}{10}D_{10} - \frac{4}{9}D_{11} + \frac{1}{9}D_{12} + \frac{1}{9}D_{13} - \frac{1}{36}D_{14} - \frac{16}{45}D_{15} \\
\widehat{D}_{3_{S_1-{}^3D_1}} &= -\frac{2\sqrt{2}}{3}D_{11} - \frac{\sqrt{2}}{6}D_{12} - \frac{\sqrt{2}}{6}D_{13} - \frac{\sqrt{2}}{24}D_{14} \\
D_{3_{S_1-{}^3D_1}} &= -\frac{14\sqrt{2}}{9}D_{11} + \frac{\sqrt{2}}{18}D_{12} + \frac{\sqrt{2}}{18}D_{13} - \frac{7\sqrt{2}}{72}D_{14} + \frac{2\sqrt{2}}{9}D_{15} \\
D_{1_{D_2}} &= \frac{8}{15}D_1 + \frac{1}{30}D_2 - \frac{2}{15}D_3 - \frac{2}{15}D_4 - \frac{8}{5}D_5 - \frac{1}{10}D_6 + \frac{2}{5}D_7 + \frac{2}{5}D_8 - \frac{8}{15}D_{11} \\
&\quad +\frac{2}{15}D_{12} + \frac{2}{15}D_{13} - \frac{1}{30}D_{14} + \frac{2}{15}D_{15} \\
D_{3_{D_2}} &= \frac{8}{15}D_1 + \frac{1}{30}D_2 - \frac{2}{15}D_3 - \frac{2}{15}D_4 + \frac{8}{15}D_5 + \frac{1}{30}D_6 - \frac{2}{15}D_7 - \frac{2}{15}D_8 \\
&\quad +\frac{2}{15}D_9 - \frac{1}{30}D_{10} + \frac{4}{5}D_{11} - \frac{1}{5}D_{12} - \frac{1}{5}D_{13} + \frac{1}{20}D_{14} + \frac{4}{15}D_{15} \\
D_{3_{P_2}} &= -\frac{4}{3}D_1 + \frac{1}{12}D_2 - \frac{4}{3}D_5 + \frac{1}{12}D_6 + \frac{1}{3}D_9 + \frac{1}{12}D_{10} - \frac{2}{15}D_{11} + \frac{1}{30}D_{12} \\
&\quad -\frac{1}{30}D_{13} + \frac{1}{120}D_{14} \\
D_{3_{P_2-{}^3F_2}} &= \frac{4\sqrt{6}}{15}D_{11} - \frac{\sqrt{6}}{15}D_{12} + \frac{\sqrt{6}}{15}D_{13} - \frac{\sqrt{6}}{60}D_{14}
\end{aligned}
$$

$$
\begin{aligned}
D_{3_{D_3}} &= \frac{8}{15}D_1 + \frac{1}{30}D_2 - \frac{2}{15}D_3 - \frac{2}{15}D_4 + \frac{8}{15}D_5 + \frac{1}{30}D_6 - \frac{2}{15}D_7 - \frac{2}{15}D_8 \\
&\quad -\frac{4}{15}D_9 + \frac{1}{15}D_{10} - \frac{2}{15}D_{15}
\end{aligned} \tag{126}
$$

References

[1] H. Yukawa, Proc. Phys. Math. Soc. Japan **17**, 48 (1935).

[2] Prog. Theor. Phys. (Kyoto), Supplement **3** (1956).

[3] M. Taketani, S. Machida, and S. Onuma, Prog. Theor. Phys. (Kyoto) **7**, 45 (1952).

[4] K. A. Brueckner and K. M. Watson, Phys. Rev. **90**, 699; **92**, 1023 (1953).

[5] A. R. Erwin *et al.*, Phys. Rev. Lett. **6**, 628 (1961); B. C. Maglić *et al.*, *ibid.* **7**, 178 (1961).

[6] Prog. Theor. Phys. (Kyoto), Supplement **39** (1967); R. A. Bryan and B. L. Scott, Phys. Rev. **177**, 1435 (1969); M. M. Nagels *et al.*, Phys. Rev. D **17**, 768 (1978).

[7] R. Machleidt, Adv. Nucl. Phys. **19**, 189 (1989).

[8] V. G. J. Stoks *et al.*, Phys. Rev. C **49**, 2950 (1994).

[9] R. Machleidt, Phys. Rev. C **63**, 024001 (2001).

[10] A. D. Jackson, D. O. Riska, and B. Verwest, Nucl. Phys. **A249**, 397 (1975).

[11] R. Vinh Mau, in *Mesons in Nuclei*, edited by M. Rho and D. H. Wilkinson (North-Holland, Amsterdam, 1979), Vol. I, p. 151.

[12] M. Lacombe, B. Loiseau, J. M. Richard, R. Vinh Mau, J. Côté, P. Pires, and R. de Tourreil, Phys. Rev. C **21**, 861 (1980).

[13] R. Machleidt, K. Holinde, and Ch. Elster, Phys. Rep. **149**, 1 (1987).

[14] F. Myhrer and J. Wroldsen, Rev. Mod. Phys. **60**, 629 (1988).

[15] D. R. Entem, F. Fernandez, and A. Valcarce, Phys. Rev. C **62**, 034002 (2000).

[16] G. H. Wu, J. L. Ping, L. J. Teng, F. Wang, and T. Goldman, Nucl. Phys. **A673**, 273 (2000).

[17] S. Weinberg, Physica **96A**, 327 (1979).

[18] S. Weinberg, Phys. Lett. B **251**, 288 (1990); Nucl. Phys. **B363**, 3 (1991); Phys. Lett. B **295**, 114 (1992).

[19] C. Ordóñez, L. Ray, and U. van Kolck, Phys. Rev. Lett. **72**, 1982 (1994); Phys. Rev. C **53**, 2086 (1996).

[20] U. van Kolck, Prog. Part. Nucl. Phys. **43**, 337 (1999).

[21] L. S. Celenza *et al.*, Phys. Rev. C **46**, 2213 (1992); C. A. da Rocha *et al.*, *ibid.* **49**, 1818 (1994); D. B. Kaplan *et al.*, Nucl. Phys. **B478**, 629 (1996).

[22] N. Kaiser, R. Brockmann, and W. Weise, Nucl. Phys. **A625**, 758 (1997).

[23] N. Kaiser, S. Gerstendörfer, and W. Weise, Nucl. Phys. **A637**, 395 (1998).

[24] E. Epelbaum *et al.*, Nucl. Phys. **A637**, 107 (1998); **A671**, 295 (2000).

[25] D. R. Entem and R. Machleidt, Phys. Lett. B **524**, 93 (2002).

[26] D. R. Entem and R. Machleidt, Phys. Rev. C **66**, 014002 (2002).

[27] D. R. Entem and R. Machleidt, Phys. Rev. C **68**, 041001 (2003).

[28] R. Machleidt and D. R. Entem, J. Phys. G: Nucl. Phys. **31**, S1235 (2005).

[29] P. F. Bedaque and U. van Kolck, Ann. Rev. Nucl. Part. Sci. **52**, 339 (2002).

[30] S. Scherer and M. R. Schindler, arXiv:hep-ph/0505265.

[31] Review of Particle Physics, J. Phys. G: Nucl. Part. Phys. **33**, 1 (2006).

[32] S. Coleman, J. Wess, and B. Zumino, Phys. Rev. **177**, 2239 (1969); C. G. Callan, S. Coleman, J. Wess, and B. Zumino, *ibid.* **177**, 2247 (1969).

[33] J. Gasser and H. Leutwyler, Ann. Phys. **158**, 142 (1984).

[34] J. Gasser, M. E. Sainio, and A. Švarc, Nucl. Phys. **B307**, 779 (1988).

[35] V. Bernard, N. Kaiser, and U.-G. Meißner, Int. J. Mod. Phys. E **4**, 193 (1995).

[36] N. Fettes, U.-G. Meißner, M. Mojžiš, and S. Steininger, Ann. Phys. (N.Y.) **283**, 273 (2000); **288**, 249 (2001).

[37] N. Fettes, U.-G. Meißner, and S. Steiniger, Nucl. Phys. **A640**, 199 (1998).

[38] N. Kaiser, Phys. Rev. C **61**, 014003 (1999); **62**, 024001 (2000).

[39] U. van Kolck, Phys. Rev. C **49**, 2932 (1994).

[40] E. Epelbaum *et al.*, Phys. Rev. C **66**, 064001 (2002).

[41] N. Kaiser, Phys. Rev. C **64**, 057001 (2001).

[42] N. Kaiser, Phys. Rev. C **65**, 017001 (2002).

[43] R. Blankenbecler and R. Sugar, *Phys. Rev.* **142**, 1051 (1966).

[44] This section closely follows Ref. [26].

[45] G. Q. Li and R. Machleidt, Phys. Rev. C **58**, 3153 (1998).

[46] V. Stoks, R. Timmermans, and J. J. de Swart, Phys. Rev. C **47**, 512 (1993).

[47] R. A. Arndt, R. L. Workman, and M. M. Pavan, Phys. Rev. C **49**, 2729 (1994).

[48] P. Büttiker and U.-G. Meißner, Nucl. Phys. **A668**, 97 (2000).

[49] V. G. J. Stoks, R. A. M. Klomp, M. C. M. Rentmeester, and J. J. de Swart, Phys. Rev. C **48**, 792 (1993).

[50] R. A. Arndt, I. I. Strakovsky, and R. L. Workman, SAID, Scattering Analysis Interactive Dial-in computer facility, George Washington University (formerly Virginia Polytechnic Institute), solution SM99 (Summer 1999); for more information see, e. g., R. A. Arndt, I. I. Strakovsky, and R. L. Workman, Phys. Rev. C **50**, 2731 (1994).

[51] In fact, preliminary calculations, which take an important class of diagrams of order five into account, indicate that the N^4LO contribution may prevailingly be repulsive (N. Kaiser, private communication).

[52] G. E. Brown and A. D. Jackson, *The Nucleon-Nucleon Interaction*, (North-Holland, Amsterdam, 1976).

[53] N. Kaiser, Phys. Rev. C **63**, 044010 (2001).

[54] K. Erkelenz, R. Alzetta, and K. Holinde, Nucl. Phys. **A176**, 413 (1971); note that there is an error in equation (4.22) of this paper where it should read

$$^{-}W^{J}_{LS} = 2qq' \, \frac{J-1}{2J-1} \left[A^{J-2,(0)}_{LS} - A^{J(0)}_{LS} \right]$$

and

$$^{+}W^{J}_{LS} = 2qq' \, \frac{J+2}{2J+3} \left[A^{J+2,(0)}_{LS} - A^{J(0)}_{LS} \right] .$$

[55] E. E. Salpeter and H. A. Bethe, *Phys. Rev.* **84**, 1232 (1951).

[56] The 1999 NN data base is defined in Ref. [9].

[57] E. Epelbaum, W. Glöckle, and U.-G. Meißner, Eur. Phys. J. **A19**, 401 (2004).

[58] M. Walzl *et al.*, Nucl. Phys. **A693**, 663 (2001).

[59] U. van Kolck *et al.*, Phys. Rev. Lett. **80**, 4386 (1998).

[60] E. Epelbaum, W. Glöckle, and U.-G. Meißner, Nucl. Phys. A747, 362 (2005).

[61] R. B. Wiringa *et al.*, Phys. Rev. C **51**, 38 (1995).

[62] A. Huber *et al.*, Phys. Rev. Lett. **80**, 468 (1998).

[63] A. Nogga, P. Navratil, B. R. Barrett, and J. P. Vary, Phys. Rev. C **73**, 064002 (2006).

[64] A. Nogga *et al.*, Nucl. Phys. **A737**, 236 (2004).

[65] P. Navratil, V. G. Gueorguiev, J. P. Vary, W. E. Ormand, and A. Nogga, arXiv:nucl-th/0701038.

[66] U.-G. Meißner, Proc. 18th International Conference on Few-Body Problems in Physics, Santos, SP, Brazil, August 2006, to be published in Nucl. Phys. **A**.

[67] E. Epelbaum, Phys. Lett. B **639**, 456 (2006).

[68] D. Rozpedzik *et al.*, Acta Phys. Polon. **B37**, 2889 (2006); arXiv:nucl-th/0606017.

[69] L. Coraggio *et al.*, Phys. Rev. C **66**. 021303 (2002).

[70] L. Coraggio *et al.*, Phys. Rev. C **71**. 014307 (2005).

[71] P. Navrátil and E. Caurier (2004) *Phys. Rev. C* **69** 014311.

[72] C. Forssen *et al.*, Phys. Rev. C **71**, 044312 (2005).

[73] J.P. Vary *et al.*, Eur. Phys. J. A **25** s01, 475 (2005).

[74] K. Kowalski *et al.*, Phys. Rev. Lett. **92**, 132501 (2004).

[75] D.J. Dean and M. Hjorth-Jensen (2004) *Phys. Rev.* C **69** 054320.

[76] M. Wloch *et al.*, J. Phys. G **31**, S1291 (2005); Phys. Rev. Lett. **94**, 21250 (2005).

[77] D.J. Dean *et al.*, Nucl. Phys. **752**, 299 (2005).

[78] J.R. Gour *et al.*, Phys. Rev. C **74**, 024310 (2006).

[79] S. Fujii, R. Okamato, and K. Suzuki, Phys. Rev. C **69**, 034328 (2004).

[80] K. Ermisch *et al.*, Phys. Rev. C **71**, 064004 (2005).

[81] H. Witala, J. Golak, R. Skibinski, W. Glöckle, A. Nogga, E. Epelbaum, H. Kamada, A. Kievsky, and M. Viviani, Phys. Rev. C **73**, 044004 (2006).

[82] A. Nogga, R. G. E. Timmermans, and U. van Kolck, Phys. Rev. C **72**, 054006 (2005).

[83] E. Epelbaum, U.-G. Meißner, arXiv:nucl-th/0609037.